Role of dust direct radiative effect on the tropical rainbelt over Middle East and North Africa: A high resolution AGCM study

AGU PUBLICATIONS

JGR

Journal of Geophysical Research: Atmospheres

RESEARCH ARTICLE

10.1002/2015JD023122

Key Points:
- High-resolution AGCM simulations with and without dust are compared over MENA
- Local Hadley circulation, AEJ, and monsoon strengthen and shift northward
- A consistent strengthening and shift of the tropical rain belt is predicted

Correspondence to:
H. K. Bangalath,
hamzakunhu.bangalath@kaust.edu.sa

Citation:
Bangalath, H. K., and G. Stenchikov (2015), Role of dust direct radiative effect on the tropical rain belt over Middle East and North Africa: A high-resolution AGCM study, *J. Geophys. Res. Atmos.*, *120*, doi:10.1002/2015JD023122.

Received 16 JAN 2015
Accepted 20 APR 2015
Accepted article online 25 APR 2015

Role of dust direct radiative effect on the tropical rain belt over Middle East and North Africa: A high-resolution AGCM study

Hamza Kunhu Bangalath[1] and Georgiy Stenchikov[1]

[1] Earth Science and Engineering, King Abdullah University of Science and Technology, Thuwal, Saudi Arabia

Abstract To investigate the influence of direct radiative effect of dust on the tropical summer rain belt across the Middle East and North Africa (MENA), the present study utilizes the high-resolution capability of an Atmospheric General Circulation Model, the High-Resolution Atmospheric Model. Ensembles of Atmospheric Model Intercomparison Project style simulations have been conducted with and without dust radiative impacts, to differentiate the influence of dust on the tropical rain belt. The analysis focuses on summer season. The results highlight the role of dust-induced responses in global- and regional-scale circulations in determining the strength and the latitudinal extent of the tropical rain belt. A significant response in the strength and position of the local Hadley circulation is predicted in response to meridionally asymmetric distribution of dust and the corresponding radiative effects. Significant responses are also found in regional circulation features such as African Easterly Jet and West African Monsoon circulation. Consistent with these dynamic responses at various scales, the tropical rain belt across MENA strengthens and shifts northward. Importantly, the summer precipitation over the semiarid strip south of Sahara, including Sahel, increases up to 20%. As this region is characterized by the "Sahel drought," the predicted precipitation sensitivity to the dust loading over this region has a wide range of socioeconomic implications. Overall, the study demonstrates the extreme importance of incorporating dust radiative effects and the corresponding circulation responses at various scales, in the simulations and future projections of this region's climate.

1. Introduction

Mineral dust is one of the most abundant aerosol species in the atmosphere by mass. Results from 16 models examined by the Aerosol Comparisons between Observations and Models (AeroCom) project [*Kinne et al.*, 2005; *Textor et al.*, 2006] show that, annually, there are about 700 to 4000 trillion grams (Tg) of dust influx into the atmosphere. As a major component of the atmospheric aerosol, dust significantly influences the energy balance of the climate system by perturbing the atmospheric radiative fluxes. By scattering and absorbing both solar and planetary radiation along with the emission of thermal infrared radiation, dust induces a direct radiative effect on climate [e.g., *Miller and Tegen*, 1998; *Sokolik and Toon*, 1996; *Kaufman et al.*, 2001]. As a rapid atmospheric adjustment to these radiative perturbations, dust also causes a semidirect aerosol effect [*Hansen et al.*, 1997]. This process, which refers to the absorption of solar radiation and the consequent warming of the atmosphere, leads to changes in cloud cover and liquid water path. Dust also causes indirect radiative effect on climate by modifying the microphysical and radiative properties of clouds by serving as cloud condensation nuclei [e.g., *Forster et al.*, 2007; *Levin et al.*, 1996; *Rotstayn and Lohmann*, 2002].

Over the past few decades, considerable attention has been devoted to the role of dust-induced direct radiative effect on climate [e.g., *Sokolik and Toon*, 1996; *Ackerman and Chung*, 1992; *Miller and Tegen*, 1998]. Several modeling studies have already been conducted to explore the influence of direct radiative effect of dust on the climate, using models with various complexities ranging from simplified conceptual models to comprehensive earth system models [e.g., *Miller and Tegen*, 1999, 1998; *Yoshioka et al.*, 2007; *Perlwitz et al.*, 2001; *Lau et al.*, 2009; *Yue et al.*, 2010; *Milton et al.*, 2008]. However, irrespective of the general agreement on globally averaged values, significant regional disparities are evident in both magnitude and sign of the climate responses among these studies. A typical example of the regional disparity is the contrasting response of the tropical rain belt of Africa, especially over Sahel region, predicted from various modeling studies. Many of them predicted an increase in precipitation over Sahel [e.g., *Lau et al.*, 2009; *Yue et al.*, 2011a; *Miller et al.*, 2004a] in response to dust radiative effect, while others predicted a decrease in precipitation [e.g., *Yoshioka et al.*, 2007; *Yue et al.*, 2011b]. The disagreement may arise from various sources of uncertainties spanning from those associated with the difference in dust optical properties to the ability of models to resolve regional circulation features.

Dust in the atmosphere is not uniformly distributed in space as well as in time. Spatially, the dust loading is mainly confined to the dry subtropics associated with major deserts, among which North African and Arabian deserts are the most prominent dust source regions, accounting for more than half of the global dust emission [*Prospero et al.*, 2002]. It has already been demonstrated that the climate response to such spatially inhomogeneous forcing is not necessarily collocated with the forcing [e.g., *Mitchell et al.*, 1995; *Shindell and Faluvegi*, 2009; *Shindell et al.*, 2010]. Rather, the response could extend well beyond the forcing location. Tropical atmosphere is especially efficient in adjusting and redistributing localized forcings throughout the tropics because of its large Rossby Radius of deformation, compared to midlatitude [*Yu and Neelin*, 1997]. Unlike the midlatitudes, where the poleward heat transport is achieved by transient baroclinic eddies and stationary waves, large-scale overturning circulations function as heat-transporting mechanisms in the tropics [e.g., *Trenberth and Solomon*, 1994]. Regional climate in the tropics thus greatly depends on the strength and spatiotemporal extent of the global-scale overturning circulations such as Hadley and Walker circulations along with synoptic-scale circulations such as Jet streams and monsoons. As these circulations determine the sequence of weather events, they ultimately define the climatic regimes of a given region [*Giorgi and Mearns*, 1991]. Therefore, it is essential to incorporate not only the regional circulation features but also the global circulation responses, to study the regional climate response to dust forcing. However, the coarser spatial resolution of conventional General Circulation Models (GCM) and the forced boundary conditions in the Regional Climate Models (RCM) were the main hurdles in modeling and analyzing these aspects [*Sud et al.*, 2009]. The majority of modeling studies that explored the influence of mineral dust radiative forcing on the climate used coarse resolution GCMs [e.g., *Miller and Tegen*, 1998; *Yoshioka et al.*, 2007; *Perlwitz et al.*, 2001; *Lau et al.*, 2009; *Yue et al.*, 2011b], though there are a few studies using RCMs [e.g., *Ahn et al.*, 2007; *Konare et al.*, 2008; *Solmon et al.*, 2008]. On one hand, RCMs offer the advantage of a sufficient resolution for regional climate sensitivity studies but with the caveat of lacking two-way interaction between regional and global scale responses to dust. On the other hand, GCM experiments are constrained by their coarse resolution to analyze the regional climate responses, though they incorporate the expansive representation of dust-climate interaction. In this context, the current research exploits the high spatial resolution capabilities of an Atmospheric General Circulation Model (AGCM), High-Resolution Atmospheric Model (HiRAM), developed at the National Oceanic and Atmospheric Administration (NOAA) Geophysical Fluid Dynamics Laboratory (GFDL), to investigate the dust direct radiative effect on the Middle East and North Africa (MENA) tropical rain belt. Global simulations have been conducted at a spatial resolution of 25 km, which ensure an ample resolution for regional climate sensitivity analysis in conjunction with the ability to account for global and regional responses to dust direct radiative effect. More specifically, our high-resolution simulations provide a unique opportunity to examine, how the dust-induced circulation anomalies at various scales influence regional climate. To the best of the authors' knowledge, there are few published results on dust-climate interaction using a GCM at a spatial resolution of about 25 km or better and, in this sense, this study is a forerunner.

The effect of dust on the tropical rain belt in the MENA region is of great interest due primarily to the fact that global dust loading is mainly confined to the close proximity, specifically to the north of the rain belt. Furthermore, the semiarid strip across the tropical Africa, between the dry Sahara desert and the moist tropical forest, is one of the most vulnerable regions to climate variability and changes [e.g., *Dai et al.*, 2004; *Held et al.*, 2005; *Zeng*, 2003]. The western part of this strip is generally referred in the climate literature as "Sahel." The Sahel climate greatly depends on the strength and seasonal march of the tropical rain belt [e.g., *Sultan and Janicot*, 2000; *Lamb*, 1978; *Janicot*, 1992a]. Succession of dry and wet years is a characteristic feature of the Sahelian climate, where a prolonged drought commenced in the late 1960s and continued until the 1990s. This prolonged drought is considered to be one of the largest climate variations recorded in the twentieth century [*Dai et al.*, 2004; *Hulme*, 1996]. Dust radiative forcing and feedback was proposed as one of the possible mechanisms for these variabilities in the Sahel climate [*Brooks and Legrand*, 2000; *Prospero and Lamb*, 2003; *Yoshioka et al.*, 2007; *Nicholson*, 2000], which emphasizes the significant role of dust radiative effects in the region's climate. Similarly, eastern equatorial Africa is noted for extreme climate variability, with severe droughts and massive floods in alternate years [*Nicholson*, 2014a, 2014b]. Therefore, dust-induced changes in climate are of great importance in this region.

Conventionally, the mean climate and its variability in equatorial Africa is explained based on the strength and the seasonal march of the rain belt or the Intertropical Convergence Zone (ITCZ). Many of the previous studies linked the Sahel drought to an anomalous southward shift of ITCZ [*Janicot*, 1992b, 1992a; *Lamb*, 1978; *Lamb and Peppler*, 1992] from its climatological mean summer position. By comparing simulations from 22 coupled

GCMs, conducted for the Intergovernmental Panel on Climate Change (IPCC) Fourth Assessment Report (AR4), *Suzuki* [2011] showed that the seasonal march of the ITCZ over Africa is a robust phenomenon unlike that over other regions and has the least intermodel difference in ITCZ. Nonetheless, the terms "ITCZ" and "tropical rain belt" have been treated synonymously in many of these previous studies. Recent studies [e.g., *Nicholson*, 2009] showed that the ITCZ, which is classically defined as a zone of surface wind convergence, is effectively detached from the systems that produce much of the tropical rainfall over West Africa. *Žagar et al.* [2011] also showed that the ITCZ defined by precipitation maxima and that defined by wind convergence are not collocated over land. The bulk of the rainfall over tropical Africa is associated with a deep core of ascent lying between the African Easterly Jet (AEJ) and Tropical Easterly Jet (TEJ), which is far south of the location of the ITCZ defined by wind convergence [*Nicholson*, 2009]. Following these studies, the current study distinguishes between "ITCZ" and "rain belt," where the former represents the loci of meridional wind convergence and the latter represents the belt of maximum precipitation. Apart from the upper air jets, low-level synoptic-scale features such as West African Monsoon (WAM) over western Africa and the convergence between Indian Summer Monsoon (ISM) circulation with unstable air from the Congo, which forms Congo Air Boundary (CAB) in the eastern part of the continent, have also been identified as potential rain-producing mechanisms in the region. Again, to better predict the MENA tropical rain belt response to dust radiative effect, it is essential to account for both regional and global circulation responses.

It is important to note that in our Atmospheric Model Intercomparison Project (AMIP)-style simulations, sea surface temperature (SST) is prescribed with observed values. Such simulations fail to account for the potentially important SST feedback on the hydrologic cycle. However, the present study specifically investigates the atmosphere-only response to dust radiative effects. The atmospheric responses from the AMIP-style simulations are more representative for time periods when ocean response is delayed due to thermal inertia [*Allen and Sherwood*, 2011; *Lau et al.*, 2006; *Randles et al.*, 2013]. Since the observed SST comprises the anomalies caused by the physical-world forcings, simulations will be able to capture the features which usually cannot be exactly reproduced with coupled GCM experiments (e.g., El Niño frequency and magnitude) [*Ott et al.*, 2010; *Randles et al.*, 2013]. The current analysis focuses only on the boreal summer (June-July-August, JJA) season, as it is the season of maximum precipitation and dust loading in the domain. It should also be noted that the present study solely focuses on the direct radiative effect of dust and does not account for its indirect effect.

The remaining part of the paper is organized as follows. A brief review of the model and a detailed description of the experiment design are included in section 2. In section 3, dust-induced impacts on the radiation, climate, and circulation are discussed. A thorough analysis of the possible roles of global- and regional-scale circulation responses in mediating the climate responses over the MENA tropical belt is included in section 4, followed by a summary in section 5.

2. Model and Experiment Design

HiRAM has been developed at GFDL based on the Atmospheric Model (AM2) [*Anderson et al.*, 2004; *Zhao et al.*, 2009]. It allows the use of fine horizontal grid spacing up to few kilometers and has an improved (compared to AM2) vertical resolution (32 levels). HiRAM employs a cubed-sphere finite-volume dynamical core [*Lin*, 2004; *Putman and Lin*, 2007] and uses a shallow convective scheme (for moist convection and stratiform cloudiness) instead of a customary deep convective parameterization. HiRAM retains most of the other parameterization modules from AM2, including radiative transfer schemes [*Schwarzkopf and Ramaswamy*, 1999; *Freidenreich and Ramaswamy*, 1999]. Here we use HiRAM at C360 (about 25 km) resolution, forced with the observed monthly SST from the Hadley Centre Sea Ice and Sea Surface Temperature (HadISST) data set [*Rayner et al.*, 2003]. The model is coupled with the new GFDL land model, LM3, as the land component. The spatial resolution of the model is in the same range as regional climate models use for climate downscaling. This allows us to study regional changes using a global model that fully accounts for interactions of regional and global scales, which is especially important in the tropics.

The aerosol concentrations including dust are precalculated using the global chemistry transport model, the Model for OZone and Related chemical Tracers (MOZART) [*Horowitz et al.*, 2003]. Overall, the predicted concentrations of aerosol are within a factor of 2 of the observed values [*Ginoux et al.*, 2006]. Dust size distribution in MOZART is discretized using eight bins with sizes from 0.1 to 10 μm. The calculations use the shortwave refractive indices from the recently estimated values from *Balkanski et al.* [2007] and longwave indices are from

Table 1. Annually Averaged DDRF

	TOA			Surface		
	Shortwave	Longwave	Net	Shortwave	Longwave	Net
Global	−0.28	+0.14	−0.14	−1.46	0.44	−1.02
MENA	−0.63	+1.31	+0.68	−12.20	+4.86	−7.33

Volz [1973]. Calculations assume 2.7% of hematite content by volume, which makes dust an efficient absorber at short wavelengths [*Balkanski et al.*, 2007]. The spatially averaged single-scattering albedo at 0.55 μm equals to 0.86.

We have conducted two HiRAM experiments for a 12 year period (1999–2010). Each of these experiments comprises three sets of ensemble members calculated from different initial conditions. The first two years are considered as the spin-up period and are omitted from the analysis. The first experiment accounts for dust radiative effect in the simulation using a prescribed seasonally varying dust loading, which is hereafter referred as "DUST" experiment. The second experiment omits the dust radiative forcing in the simulation and is referred as "NoDUST" experiment. Atmospheric response to dust forcing can then be estimated as the difference in the climate variables between these two simulations.

3. Results

3.1. Radiative Effects

In general, radiative forcing is used as a general metric to characterize the radiative impact of aerosol on climate [e.g., *Miller and Tegen*, 1998; *Yoshioka et al.*, 2007; *Perlwitz et al.*, 2001; *Lau et al.*, 2009; *Yue et al.*, 2010]. A generic definition of radiative forcing of aerosols would be the radiative flux perturbation induced by aerosols prior to any climate response [*Hansen et al.*, 2005]. Complying with this, Dust Direct Radiative Forcing (DDRF) is defined and estimated as the "net (longwave + shortwave) radiative flux (downwelling minus upwelling) difference between a state with no dust loading and that with a seasonally varying climatological dust loading, calculated with the same meteorological field, under all-sky condition," in the current research. Hence, positive values represent warming of the system, due to the presence of dust, while negative values indicate a cooling of the system. Since mineral dust aerosol is an effective absorber at short wavelength, the change in radiative fluxes within the atmosphere and at surface are equally as important as that at the top of the atmosphere [e.g., *Miller et al.*, 2004b]. Therefore, the DDRF is estimated at both the surface and top of the atmosphere (TOA). The difference between the DDRF at TOA and that at surface can be deduced as the dust-induced heating or cooling in the atmosphere, which has the potential to alter the vertical stability of the atmospheric column and temperature gradients, resulting in further circulation changes.

To estimate the instantaneous radiative flux changes due to dust loading, the model calls the radiation calculation twice at each radiation time step: one with dust influence and the other without dust influence. But only the radiation fluxes calculated with dust radiative effect feedback to the model evolution. Thus, the instantaneous radiative forcing and heating rate anomalies can be estimated as the differences in fluxes and heating rates calculated with and without the dust effect, respectively.

Table 1 shows the annual mean of DDRF in the current simulation. Globally averaged DDRF is −0.14 W/m^2 at TOA, with −0.28 W/m^2 contributions from shortwave and +0.14 W/m^2 from longwave. Surface values are larger compared to that of TOA forcing. The globally averaged annual value is −1.02 W/m^2 with a contribution of −1.46 W/m^2 from shortwave and 0.44 W/m^2 from longwave. We find that the globally averaged annual DDRF in our simulation compares well with that of the previous studies [see *Yue et al.*, 2010, Table 1]. Regionally, however, the forcing varies greatly in magnitude and even changes the sign from that of globally averaged forcing. Over MENA (0–35°N; 20°W–60°E), where the world's biggest deserts reside, averaged TOA and surface DDRF are +0.68 W/m^2 and −7.3 W/m^2, respectively. These values are 1 order of magnitude bigger than the globally averaged values and presumably make DDRF a significant contributor in the radiation budget over this region.

The spatial pattern of DDRF at TOA and at surface during the summer season are shown in Figure 1. At surface, there is a net reduction in the radiation throughout the globe with a predominant cooling over subtropical deserts and downwind of these dust source regions. However, DDRF at TOA also shows regional changes in

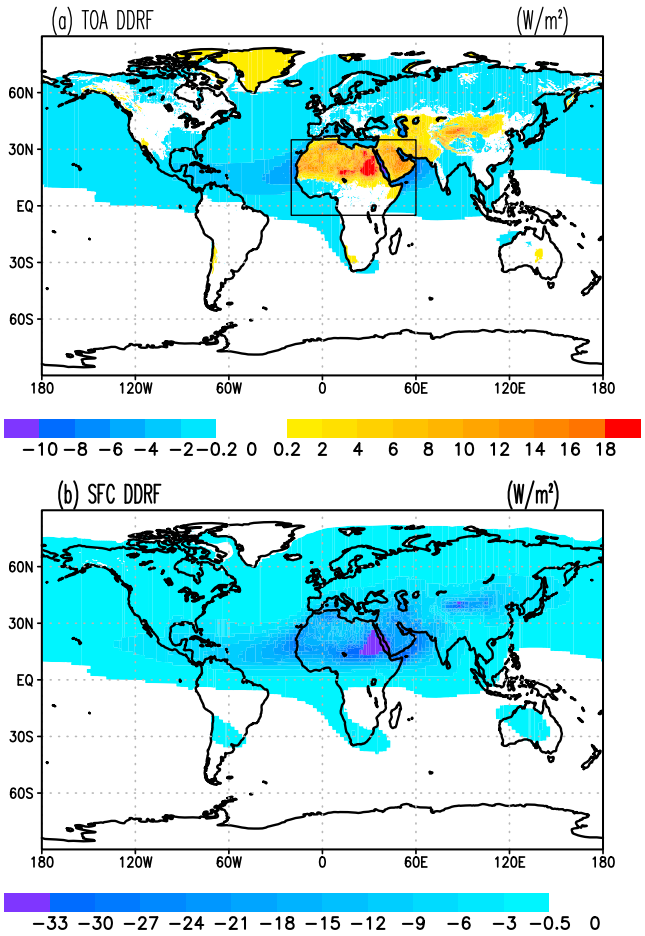

Figure 1. Mean summer (JJA) DDRF (W/m^2) in HiRAM simulations (a) at TOA and (b) at surface. Positive values denote a net warming of the system while negative indicate a net cooling, due to dust loading. The rectangle in Figure 1a marks the boundary of MENA region defined in the present study.

the sign of the forcing, in addition to the varying magnitude. Regionally, the effect is largest over deserts with high positive values and strong negative forcing over the oceans downwind of the Saharan and Arabian dust source regions such as the equatorial Atlantic Ocean, the Northern Arabian Sea, and the Red Sea. The climatologically averaged values at TOA reach about 16 W/m^2 over hot spots such as the area near Tokar Gap in Northeast Africa, whereas negative forcing reaches its maxima up to about −8 W/m^2 offshore of the western Sahara and over the Red Sea (Figure 1). At surface, the forcing is even stronger, going up to about −30 W/m^2 under the dusty regions. It has already been shown that, during dust events, locally, the values of DDRF can be more than 2 or 3 times that of the seasonal average values [e.g., *Kalenderski et al.*, 2013; *Slingo et al.*, 2006; *Jish Prakash et al.*, 2014], which makes dust-induced radiative perturbations a major component of the region's radiation budget.

In general, DDRF at TOA is smaller than that at the surface, since the TOA radiative anomaly caused by the shortwave scattering is greatly offset by the shortwave and longwave absorption in the column. At surface, both scattering and absorption alike contribute to the reduction in the net radiation and, hence, produce an intense cooling. Consequently, the difference in the DDRF between surface and TOA indicates the heating or cooling of the atmospheric column by dust [*Miller and Tegen*, 1999; *Miller et al.*, 2004b; *Ramanathan et al.*, 2001]. Strikingly positive values of DDRF at TOA occur over MENA compared to the remaining part of the world. Both the surface albedo effect [*Chýlek and Coakley*, 1974] and dust shortwave absorption lead to a TOA positive DDRF over the bright deserts in the region.

DDRF has a strong hemispheric contrast associated with the fact that the geographical location of the major dust source regions, including major deserts, lies in the Northern Hemisphere (NH). This contrast in DDRF distribution is most evident over the MENA region. To the north of the tropical rain belt, there is an immense dust loading and corresponding radiative effect, while dust radiative effect is negligible to the south of the rain belt. This could induce interhemispheric differential heating, which presumably influences the north-south temperature gradient and the local Hadley circulation.

To expose the vertical structure of the dust-induced north-south gradient in the radiative perturbations, a latitude-height cross section of zonally averaged (20°W–60°E) dust-induced anomaly (shaded contours) in radiative heating rate (shortwave plus longwave) is plotted (Figure 2). To compare the relative importance of the dust-induced heating anomaly in the net radiation budget of the region, the net radiative heating rate is overlaid as contour lines. Dust-induced radiative heating is concentrated over the Northern Hemispheric subtropics, associated with the Sahara and Arabian deserts. The magnitude of the dust-induced heating is comparable to the values of the climatological net radiative heating rate, and the core of this heating goes up to the middle troposphere (up to 500 hPa). In effect, dust causes a strong hemispheric gradient in the net

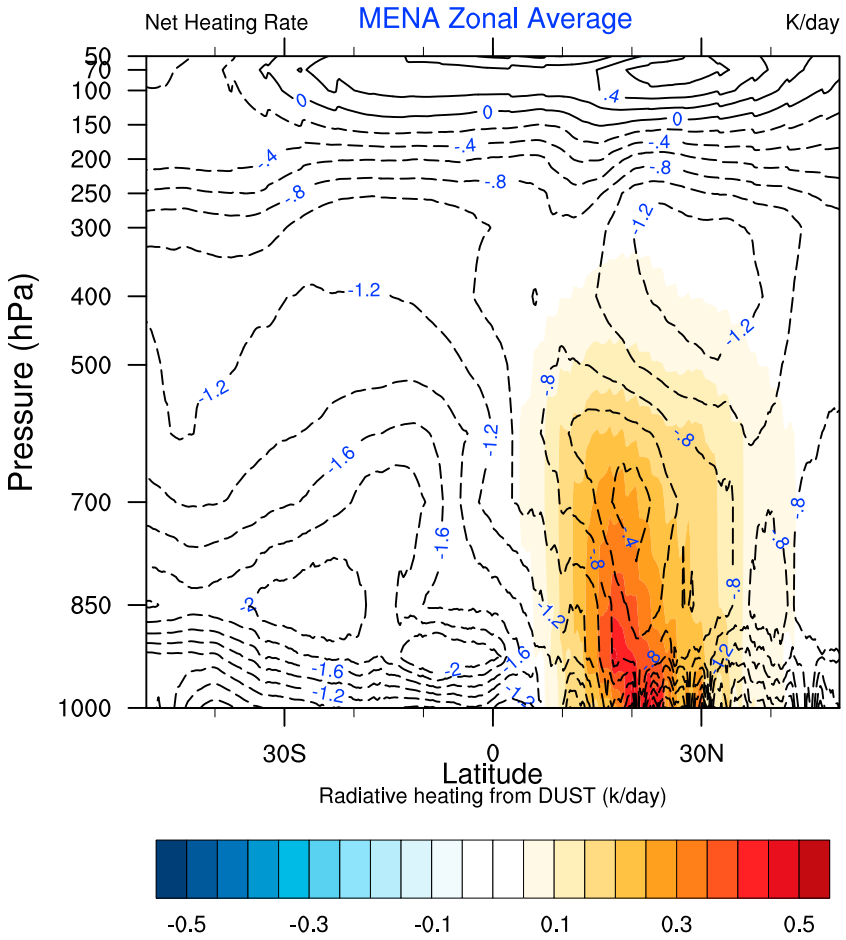

Figure 2. Latitude-height cross section of zonally averaged (20°W–60°E) climatological radiative heating rate (shortwave plus longwave) due to dust loading (shaded contours) overlaid on net radiative heating rates (contour lines) during summer (JJA)

heating rate throughout the lower-middle troposphere. Most importantly, the net radiative cooling over the northern subtropics is visibly half of that of the remaining tropics, indicating the importance of dust-induced heating in the radiative profile of this region. That is to say, the dust-induced positive heating rate can effectively reduce the net radiative cooling from the region and it can potentially act as an off-equator heating source. *Lindzen and Hou* [1988] proved that heating off the equator induces profound asymmetries in the Hadley circulation. Their simplified calculations showed that, as the heating moves off the equator, the latitude separating the two cells moves farther into the summer hemisphere. In this context, dust-induced radiative heating, asymmetrically placed over the Northern Hemispheric subtropics, is thought to alter the local Hadley circulation strength and position.

3.2. Climate Response

The climate response forced by dust has been characterized by the differences in the seasonal ensemble mean of meteorological fields between the simulations with and without dust radiative effect (DUST − NoDUST). The analysis primarily focuses on the changes in the two most important surface variables: precipitation and surface air temperature. To differentiate the probable cloud feedback on temperature, responses in cloud amount have also been analyzed. A statistical significance of the response is estimated at 95% confidence for all of these variables, using the two-tailed Student's *t* test. The statistically significant areas are marked by hatching in the figures.

The spatial patterns of the mean summer precipitation from the Global Precipitation Climatology Project (GPCP) [*Adler et al.*, 2003], HiRAM-simulated ensemble mean summer precipitation, and its response to dust forcing are shown in Figures 3a–3c, respectively. Model-averaged precipitation (Figure 3b) captures the

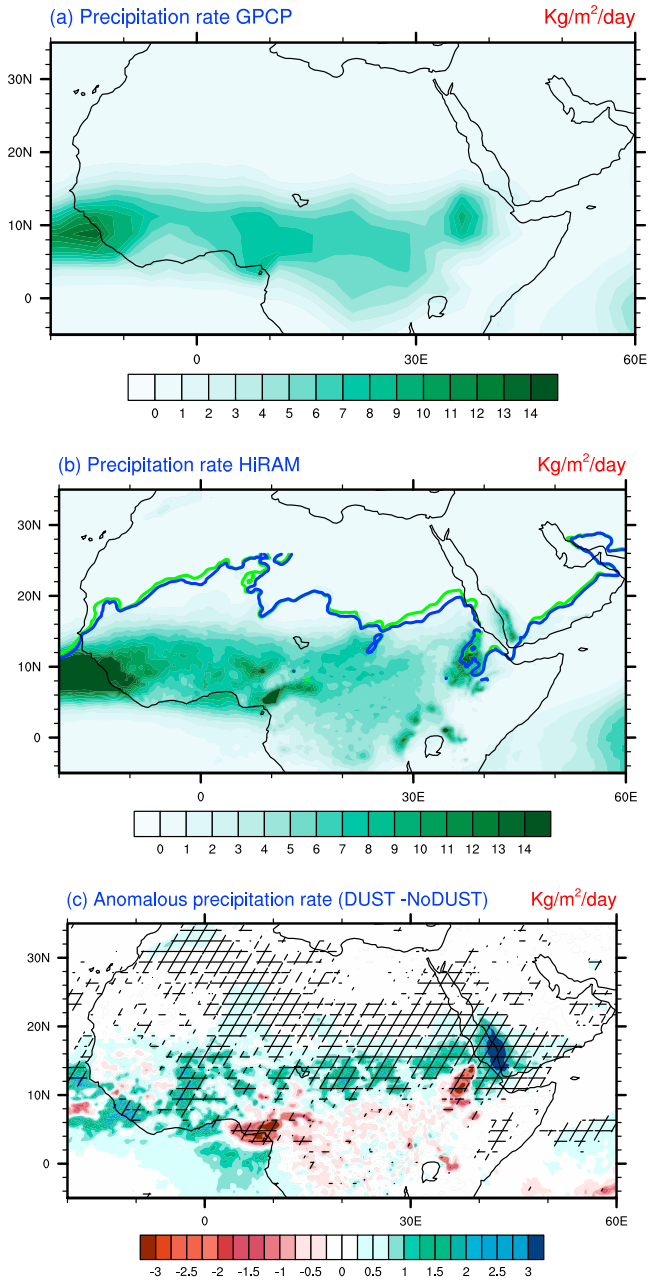

Figure 3. (a) Observed mean summer climatology (2000 to 2009) of precipitation rate from GPCP. (b) Simulated mean summer(JJA) climatology of precipitation rate (kg/m^2/d). Zero meridional wind contours between 5°S and 20°N are overlaid to show the location of ITCZ as the loci of meridional wind convergence, where thick green contours are for the ITCZ in the "DUST" simulation and the thick blue contours are for that in "NoDUST" simulation. (c) Simulated precipitation response (kg/m^2/d) to DDRF, estimated as the difference between the simulation with dust and simulation without dust (DUST − NoDUST). The hatched areas are regions of statistically significant (Student's *t* test) precipitation difference at 95% level.

key features of the observed precipitation climatology (Figure 3a) quite realistically, especially the strength and shape of the tropical rain belt across this region. Additionally, the local precipitation maxima associated with the orographic features are better represented in HiRAM simulations, due to its high spatial resolution. To demonstrate the location of ITCZ defined by wind convergence, zero meridional wind contours between 5°S and 20°N are overlaid on the mean precipitation (Figure 3b). As previously noted by *Nicholson* [2009], the ITCZ and the tropical rain belts are completely detached and the separation even goes up to about 1000 km in West Africa. A slight northward shift of ITCZ is also predicted in response to dust radiative effect (see solid blue and green contours in Figure 3b). However, the shift in ITCZ position is larger (about 2° latitude) in East Africa, compared to West Africa and the Middle East (less than 1°).

A statistically significant precipitation enhancement is predicted in the northern half of the tropical rain belt (Figure 3c), as a response to dust radiative effect. Conversely, the precipitation weakens in the southern part of the belt, though the reduction is not statistically significant everywhere. This makes a north-south dipole structure in response, indicating a possible northward shift of the local Hadley cell, which is confirmed hereinafter. However, over West Africa, the dipolar response pattern is not that apparent; instead, a widespread enhancement is predicted throughout the tropics. This could be attributed to the feedback from WAM circulation response, which has dominant zonal flow that covers the entire tropical lower troposphere in West Africa. This response is consistent with the "Elevated Heat Pump" (EHP) mechanism proposed for the monsoon intensification [*Lau et al.*, 2006, 2009], in response to dust radiative effects. By this mechanism, the warmed air in the elevated dust layer over West Africa and the eastern Atlantic rises and spawns a large-scale onshore flow carrying moist air from the eastern Atlantic and the Gulf of Guinea. This enhanced onshore moisture flow increases the cloudiness and rainfall during WAM season, throughout the West African tropics.

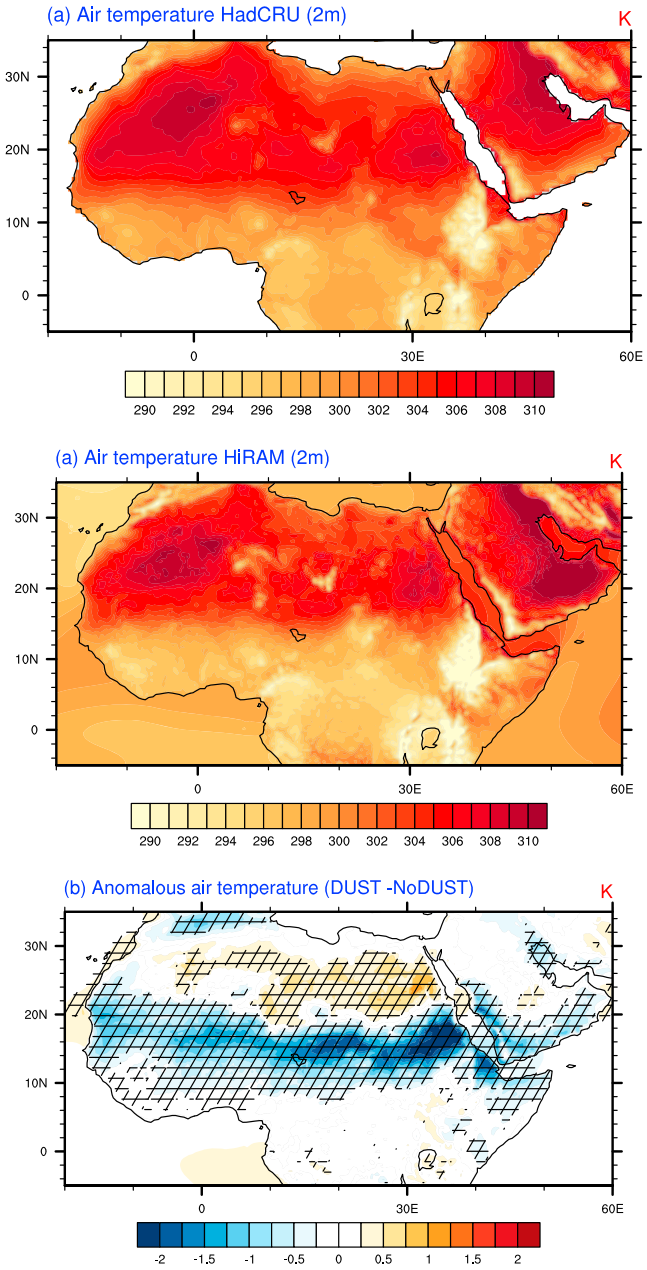

Figure 4. (a) Observed mean summer climatology (2000 to 2009) of air temperature (2 m) from HadCRU. (b) Simulated mean summer(JJA) climatology of 2 m temperature (K). (c) Simulated 2 m temperature (K) response to DDRF, estimated as the difference between the simulation with dust and simulation without dust (DUST − NoDUST). The hatched areas are regions of statistically significant (Student's *t* test) temperature difference at 95% level.

The predicted precipitation response is about 1.5 kg/m^2/d, which is about 20% of the mean summer precipitation, especially in the semiarid strip between Sahara and the tropical forest, including the Sahel region. This area is climatically very sensitive and ecologically vulnerable and is characterized by strong climatic variations and an irregular rainfall that ranges between 200 mm and 600 mm annually with coefficients of variation ranging from 15 to 30% [*Fox and Rockström*, 2003]. The predicted precipitation response to dust forcing is thus crucial for this region.

Even though the precipitation response around the rain belt has a dipole pattern, in general, there are some "hot spots" with strikingly anomalous responses. A statistically significant intense weakening of precipitation, up to about 3 kg/m^2/d, is observed along the eastern extent of CAB (over the Ethiopian Highlands), the northeast directed convergence zone between ISM circulation and unstable air from the Congo. Another hot spot is the southwestern tip of the Arabian Peninsula, where the Tokar gap wind jet interacts with Asir escarpment mountain on the western coast of Arabia. The precipitation enhancement is about 4 kg/m^2/d, which is about 50% of the mean precipitation over this region. Another hot spot in response is over the climatological summer precipitation maxima over the Cameroon highlands and the nearby coast, where the WAM circulation interacts with the highlands. All these areas are, climatologically, very well distinguished as precipitation maxima regions during boreal summer, and the orographic precipitation is the major contributor to the mean rainfall in all of these three regions. These locally amplified precipitation responses emphasize the importance of high-resolution modeling for assessing regional/local sensitivity to a certain spatially heterogenous forcing, as in our case.

The observed mean summer air temperature climatology from the UK Met Office Hadley Centre and the University of East Anglia Climatic Research Unit (HadCRUT) [*Brohan et al.*, 2006], HiRAM-simulated mean summer surface air temperature, and its response to the dust radiative effect are depicted in Figures 4a–4c, respectively. In general, the model reproduces the magnitude and the pattern of spatial temperature distributions. A strong north-south gradient in the mean temperature is evident between dry Saharan desert in the north

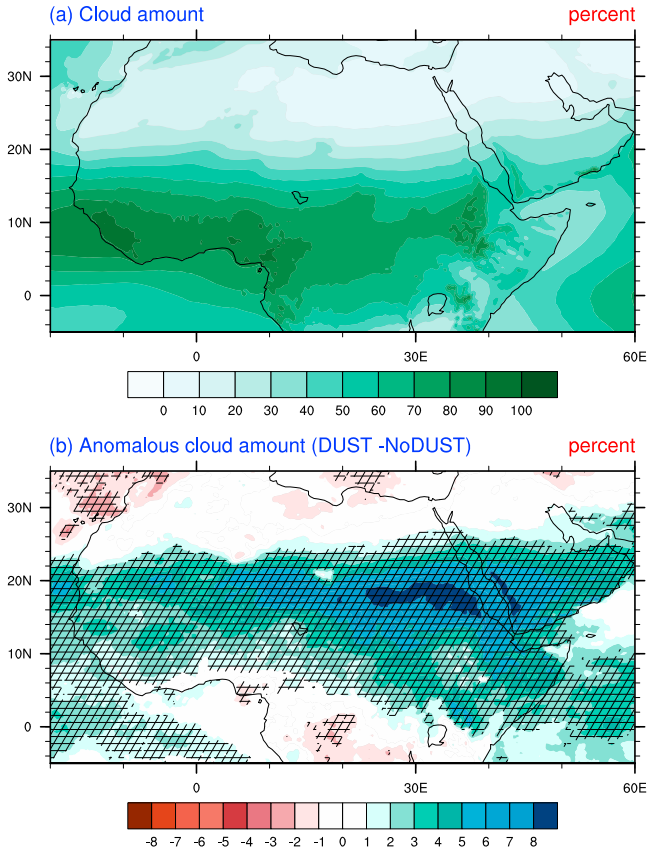

Figure 5. (a) Simulated mean summer(JJA) climatology of total cloud amount (%). (b) Simulated total cloud amount (%) response to DDRF, estimated as the difference between the simulation with dust and simulation without dust (DUST − NoDUST). The hatched areas are regions of statistically significant (Student's *t* test) temperature difference at 95% level.

and the tropical rain forest in the south (Figure 4a) and it is well represented in the simulation (Figure 4b). Similarly, the temperature maxima associated with Saharan Heat Low (SHL) and Arabian Heat Low (AHL) are also well simulated. The temperature response (Figure 4c) is mainly a reduction in temperature, which is more than 1 K to the north of the rain belt. However, there is warming, relatively less in magnitude but statistically significant, in the north part of Sahara ranging from about 0.5 K to 1 K. This positive temperature anomaly could be due to the enhanced subsidence from a strengthened local Hadley cell which is proved hereinafter. In general, temperature response is statistically more significant and has a much more consistent north-south pattern compared to the precipitation response. The intense cooling north of the rain belt, which extends to the southern Sahara, could arise from the combined influence of solar dimming due to aerosol scattering and absorption and the feedbacks from cloud, precipitation, and circulation responses. To investigate the possible cloud feedback on temperature changes, the response of cloud amount to dust forcing is analyzed (Figure 5). Note that the dust indirect effect is not included in the simulations. Thus, the cloud response could either be from the "dust semidirect" effect (thermodynamic effect), whereby absorption of radiation and the consequent warming of the atmosphere leads to reduction in cloud cover ("burning off clouds") by reducing the ambient relative humidity and evaporation of the clouds [*Hansen et al.*, 1997] and/or from the large-scale dynamic response to dust radiative effect. A widespread statistically significant enhancement in the cloudiness throughout the tropics is predicted in response to dust radiative effect (Figure 5b) and follows an inverse pattern to that of temperature. The increasing cloudiness response could potentially reduce the surface air temperature. However, the magnitude of response is comparatively higher at the northern part of the rain belt, where an increase in cloud of 8% or more is predicted. A major contribution to the increased amount of cloudiness is from low clouds (not shown). An increase in low cloud amount in response to DDRF is a counterexample to the semidirect effect ("burning off clouds") [*Perlwitz and Miller*, 2010]. Therefore, the low cloud response over Sahel could only be expected from the dominant role of global or synoptic-scale dynamic response, possibly due to an anomalous northward shift of the ascending branch of Hadley cells and the overall strengthening of the local Hadley circulation. A detailed analysis of the dynamic responses to dust forcing is presented in section 3.3.

In the context of Sahelian wet/dry episodes, *Nicholson and Grist* [2001] have noted that the enhanced precipitation over the tropical semiarid strip including Sahel, could be either due to a change in the intensity of the tropical rain belt and/or due to a latitudinal shift in the precipitation pattern. The dipole-like responses around the tropical rain belt in precipitation and temperature emphasize a possible shift in the mean meridional circulation to the north, in our case. As evident from the heating rate (Figure 2), dust loading acts as a hemispherically asymmetric off-equator heating source in the lower-middle troposphere over the MENA region and possibly strengthens and moves the ascending branch of Hadley cell farther north. To explicitly investi-

gate this, a detailed analysis of the tropospheric dynamic response to dust direct radiative effect is performed in the following sections.

3.3. Circulation Response

As a first approximation, the zonally averaged meridional picture of the dust radiative effect and the corresponding circulation response over MENA region could be summarized as an off-equatorial heating in the Northern Hemispheric lower-middle troposphere and the associated changes in the local Hadley circulation. However, the contribution of zonal circulation response to the predicted atmospheric response cannot be disregarded. To explicitly demonstrate the changes in meridional and zonal overturning circulation, it is important to divide the three-dimensional overturning into orthogonal two-dimensional overturning circulations. In other words, Hadley- and Walker-type circulations need to be separated. Conventionally, Hadley circulation is depicted by the mean meridional mass stream functions, which is calculated by vertically integrating the zonally averaged mass weighted *v* wind [*Oort and Yienger*, 1996]. This procedure is strictly defined for the global domain, and it fails for a particular longitudinal belt as mass continuity does not hold [*Trenberth et al.*, 2000; *Webster*, 2004]. Recently, *Schwendike et al.* [2014] introduced a new method for the local partitioning of the tropical overturning circulation into local Hadley and Walker circulation. In this approach, the pressure velocity omega ($\omega = \frac{Dp}{Dt}$) can be divided into components associated with meridional (ω_ϕ) and zonal (ω_λ) overturning circulations, as

$$\omega_\phi = \frac{1}{a\cos\phi}\frac{\partial}{\partial\phi}(\psi_\phi \cos\phi) = \frac{1}{a^2\cos\phi}\frac{\partial}{\partial\phi}(\cos\phi\frac{\partial\mu}{\partial\phi}) \tag{1}$$

$$\omega_\lambda = \frac{1}{a\cos\phi}\frac{\partial\psi_\lambda}{\partial\lambda} = \frac{1}{a^2\cos^2\phi}\frac{\partial^2\mu}{\partial\lambda^2} \tag{2}$$

where potential function, μ, and vector stream function, Ψ, are defined in pressure coordinate as

$$\nabla_p^2\mu = -\omega \qquad \text{and} \qquad \nabla_p\Psi = \omega, \tag{3}$$

where

$$\Psi = (\psi_\lambda, \psi_\phi) = -\nabla_p\mu \tag{4}$$

Hence, the vertical mass flux associated with two orthogonal circulations can be written as

$$m_\phi = -\omega_\phi\cos\phi/g \qquad \text{and} \qquad m_\lambda = -\omega_\lambda\cos\phi/g \tag{5}$$

Vertical mass flux associated with meridional overturning (m_ϕ) and zonal overturning (m_λ) can be portrayed as the local Hadley and Walker circulations, respectively (see *Schwendike et al.* [2014] for a detailed explanation of the method of separation).

Figure 6a shows mean summer local Hadley circulation depicted as the Hadley component of vertical mass flux, m_ϕ (kg m^{-2} s^{-1}), at 500 hPa level. Positive (negative) values indicate ascending (descending) motion. A zonally elongated band of ascending motions in the summer tropics with corresponding descent on either side of it is evident. The thick green and black contours (zero contour of m_ϕ) mark the boundary between ascending and descending branches in DUST and NoDUST simulations, respectively. The ascending branch expands northward in response to dust radiative effect. However, consistent with the surface climate response, an east-west contrast is evident in the local Hadley circulation response, with a stronger shift (about 2° of latitude) over central and East Africa. The response (DUST − NoDUST) in the strength of the vertical mass flux is displayed in Figure 6b. The ascending motion significantly enhances throughout the northern boundary between ascending and descending branches, in response to dust forcing. In contrast, the ascending motion weakens over the southern border of ascending branch, although the response is weaker. This dipolar circulation pattern of response is consistent with the predicted responses in precipitation (Figure 3).

To expose the response of regional Hadley cell (m_ϕ) aloft, a vertical cross section of m_ϕ averaged between 10°W and 60°E and its response are shown in Figures 7a and 7b, respectively. The divergent circulation in the plane (U_ϕ, ω_ϕ) is overlaid as vectors to show the flow direction and cell structure (Figure 7a). The meridional divergent wind, U_ϕ, is estimated [*Schwendike et al.*, 2014] from the definition of horizontal divergent wind in terms of velocity stream function (Ψ) as

$$U_\phi = -\frac{\partial\psi_\phi}{\partial p} \tag{6}$$

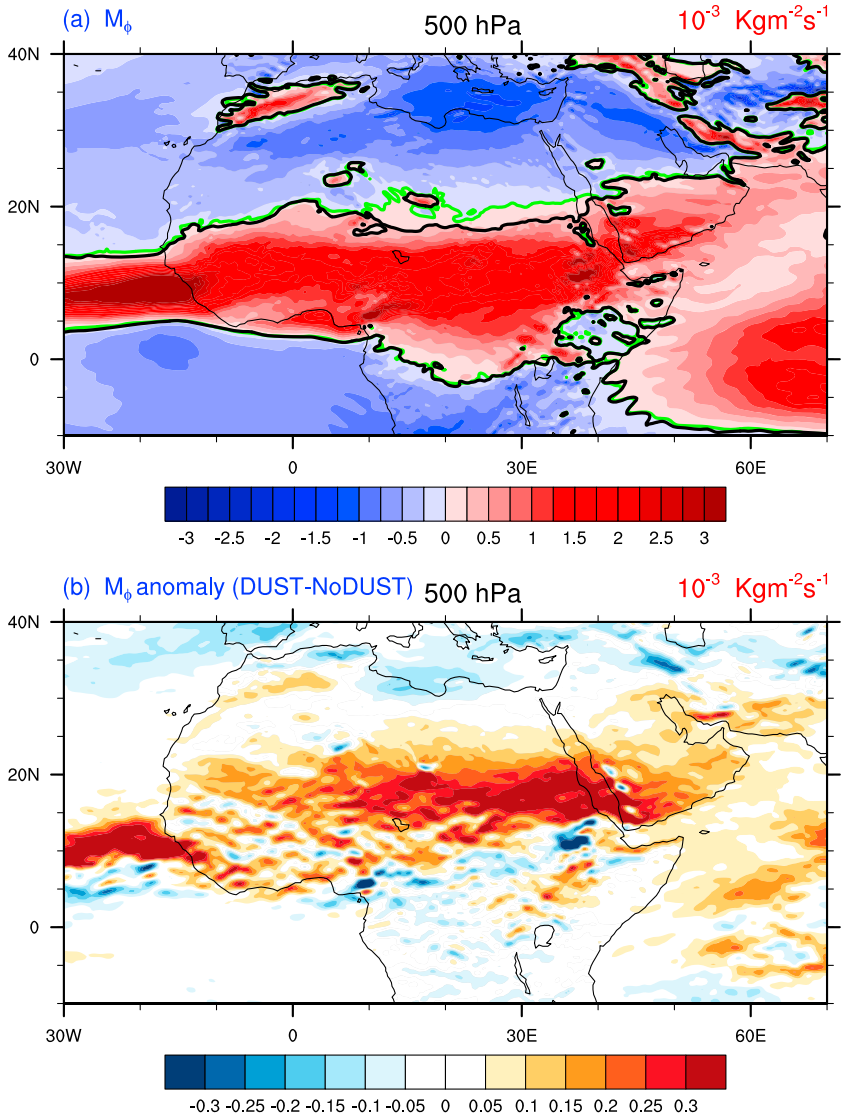

Figure 6. (a) Local Hadley circulation depicted as the vertical mass flux associated with meridional overturning, m_ϕ (kg m^{-2} s^{-1}), at 500 hPa level during summer (JJA). Positive values indicate ascending motion and vice versa. The thick green and black lines are the border (zero contour of m_ϕ) between ascending and descending branch in DUST and NoDUST simulations, respectively. (b) Response of local Hadley circulation to DDRF portrayed as the difference in m_ϕ (kg m^{-2} s^{-1}) between simulations with and without dust (DUST − NoDUST).

As the magnitude of ω_ϕ is significantly smaller compared to U_ϕ, the former is scaled by a factor of 100, in order to plot the wind vectors. A double-cell structure of Hadley circulation with a stronger winter cell is found, over MENA (Figure 7a). The ascending branch extends very much into the summer hemisphere and has a bell shape with tails of shallow ascent to either side of the main core. In response to dust radiative effect, the ascending branch strengthens in its northern border and shifts farther into the summer hemisphere (Figure 7b). Consequently, an enhanced subsidence is predicted over the southern border of the NH subsidence branch.

Similarly, mean summer local walker circulation and its response to dust radiative effect are shown in Figures 8a and 8b, respectively. The local Walker circulation is depicted as the Walker component of vertical mass flux, m_λ (kg m^{-2} s^{-1}). MENA, in general, experiences descending motion, except in regions such as the Congo basin, the northwestern part of the African continent, the Ethiopian Highlands, and the western coast of the Arabian peninsula, where m_λ is positive. The Walker circulation response to dust radiative effect (Figure 8b) is, in general, weaker compared to that of Hadley circulation. Therefore, the separation of local Hadley and Waker cell responses indicate, as expected, that the dominant response is in the meridional

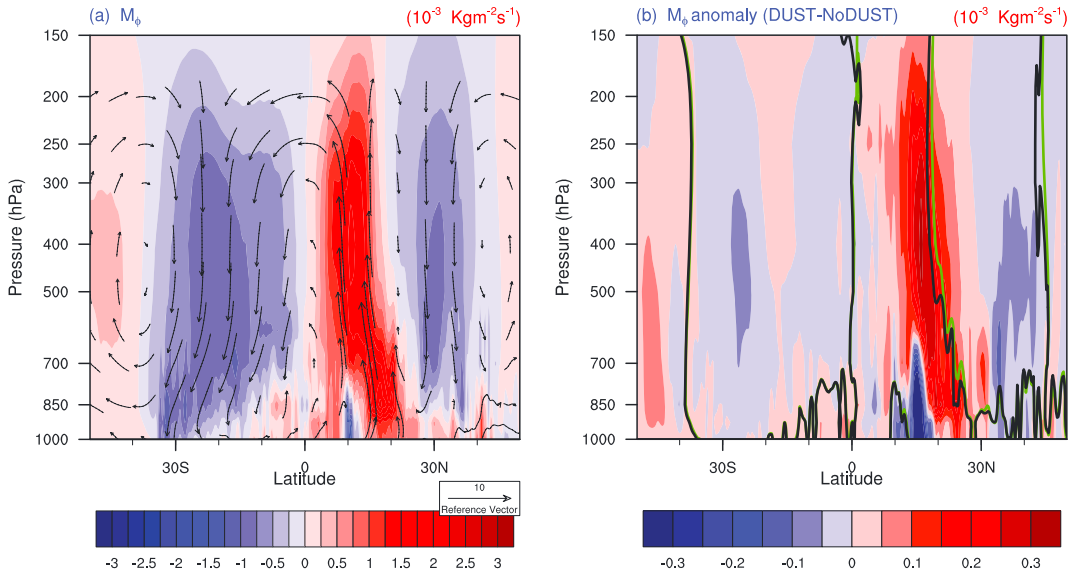

Figure 7. (a) Regional Hadley circulation over MENA. The shaded contours are the vertical mass flux associated with meridional overturning, m_ϕ (kg m^{-2} s^{-1}) averaged between 10°W and 60°E. Positive values indicate ascending motion and vice versa. Vectors represent the wind in the plane of cross section (U_ϕ, ω_ϕ). The values of ω_ϕ are scaled by multiplying to 10^2. (b) Response in the Regional Hadley circulation to DDRF, portrayed as the difference in m_ϕ (kg m^{-2} s^{-1}) between simulations with and without dust (DUST − NoDUST). The thick green and black contours are the border (zero contour of m_ϕ) between ascending and descending branch in DUST and NoDUST simulations, respectively.

direction (local Hadley circulation) as a response to meridional differential heating. Moreover, the response in Walker circulation has a mixed pattern unlike that of Hadley circulation. However, there is a strong east-west oriented dipolar response in m_λ over East Africa, specifically over the Ethiopian Highlands and the southern Red Sea. This region is one of the raising branches of global Walker circulation, and the dipolar response indicates a shift in the position of the ascending branch. A consistent east-west dipolar response is predicted in the precipitation too (Figure 3c), with a weakening of precipitation over the Ethiopian Highlands and an enhancement over the southern Red Sea and southwest coast of the Arabian Peninsula.

Apart from the zonally and meridionally overturning circulations, upper air synoptic features like AEJ and TEJ could also mediate dust-induced changes in the climate, especially in the region's precipitation. It has already been revealed that the bulk of the precipitation over tropical Africa, especially on the western part, is linked to the AEJ and TEJ and to the wave disturbances associated with them [*Nicholson*, 2009]. By comparing Sahelian wet and dry years' dynamics over west Africa, *Nicholson and Grist* [2001] showed that the two most striking differences were in the strength of TEJ and the strength and latitudinal position of AEJ. Similarly, using a combination of high-resolution dropsonde observations and model analyses, *Tompkins et al.* [2005] showed that the climatology of aerosol direct radiative effect in the simulations significantly improved the forecast of AEJ. The upper air vertical shear is a crucial factor in deciding occurrence of wet/dry mode in a given year. Since the upper air shear is greatly influenced by the relative location of the AEJ and TEJ, the latitudes of these jets are also important for the tropospheric dynamics in the region by influencing the vertical motion in general and wave activities in particular [*Nicholson et al.*, 2008]. AEJ is considered to be instrumental in providing the sufficient baroclinic and barotropic instabilities for the development of African Easterly Waves (AEW) [e.g., *Thorncroft and Hoskins*, 1994a, 1994b; *Thorncroft*, 1995]. AEW is one of the most important synoptic features of the West African summer climate. Similarly, the vertical shear associated with the AEJ is important for the growth of long-lived mesoscale convective systems (MCSs) [e.g., *Houze and Betts*, 1981], which are responsible for most of the daily rainfall events in the West African region.

To analyze the responses in AEJ to DDRF, wind speed at 600 hPa is displayed (Figure 9a). As the synoptic features, such as easterly jets and monsoon, change their positions and strength frequently, monthly fields are analyzed instead of seasonal means. For the sake of brevity, the responses shown hereafter are only for the month of August, the month having maximum precipitation in the domain. The zero contours of du/dy near the maximum wind is overlaid to depict the jet axes. The wind response to DDRF is shown as shaded

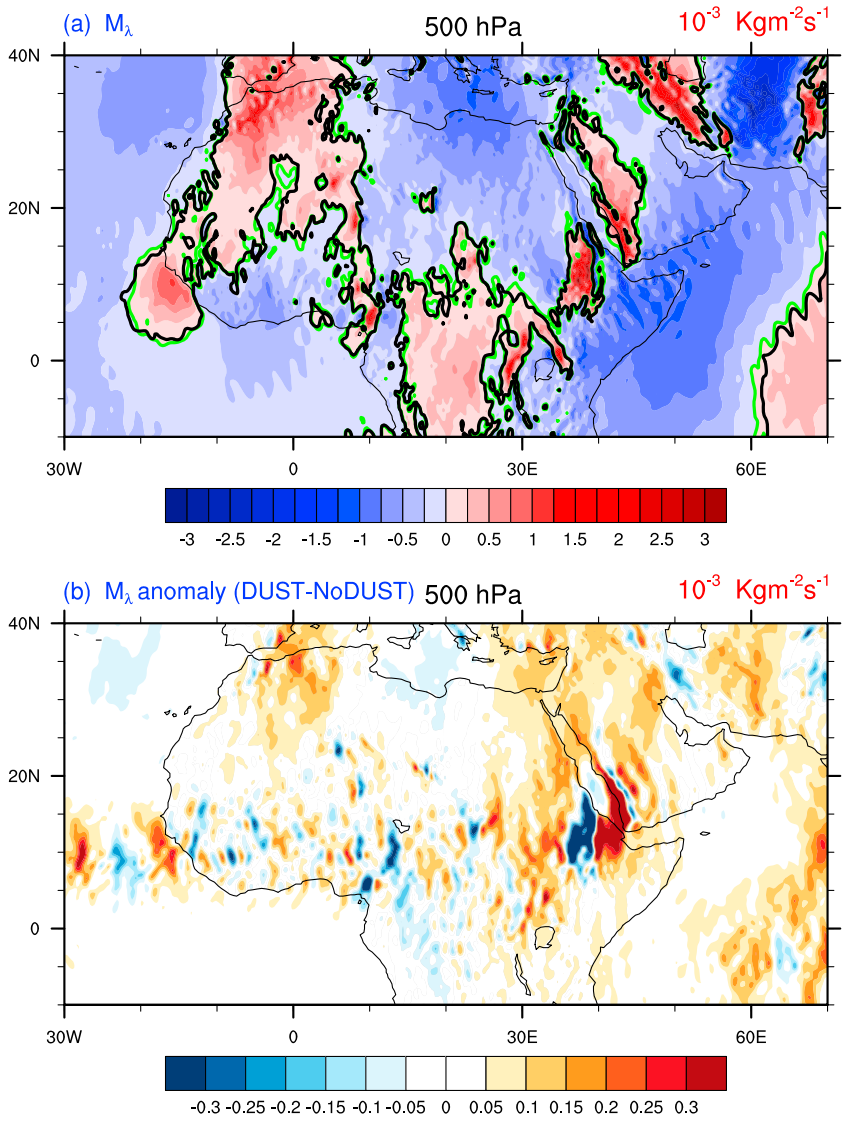

Figure 8. (a) Local Walker circulation depicted as the vertical mass flux associated with zonal overturning, m_λ (kg m^{-2} s^{-1}), at 500 hPa level during summer (JJA). Positive values indicate ascending motion and vice versa. The thick green and black lines are the border (zero contour of m_λ) between ascending and descending branch in DUST and NoDUST simulations, respectively. (b) Response of local Walker circulation to DDRF portrayed as the difference in m_λ (kg m^{-2} s^{-1}) between simulations with and without dust (DUST − NoDUST).

contours. The simulations very well capture the strength and position of both of the jets (compare *Nicholson* [2009, Figure 9]). In response to dust radiative effect, AEJ shifts northward throughout the African continent with a maximum of up to 2° latitude over East Africa. The wind speed response has a dipole structure with a statistically significant positive response to the north of the AEJ axes and a negative response to the south of it. Similar to precipitation and vertical velocity, an east-west contrast is also visible in the strength of the response with a heightened difference over East Africa. It is well known that AEJ stems from the temperature structure in the troposphere that is established in association with deep moist convection in the tropical rain belt (referred as "ITCZ" in *Thorncroft and Blackburn* [1999]) and dry convection in the lower troposphere in the Sahara; in other words, a positive meridional temperature gradient in the lower troposphere and reversal of the gradient in the middle troposphere, between Sahara and the tropical rain belt. The role of dust-induced heating gradient in the lower-middle troposphere (Figure 2), hence, is to support and strengthen the positive meridional temperature gradient in the lower troposphere. It has already been known that the latitude of the jet maxima coincides with the maximum in low-level temperature gradient [*Cook*, 1999]. The predicted northward shift in the jet axis is thus consistent with heating gradient. *Mohr and Thorncroft* [2006] showed

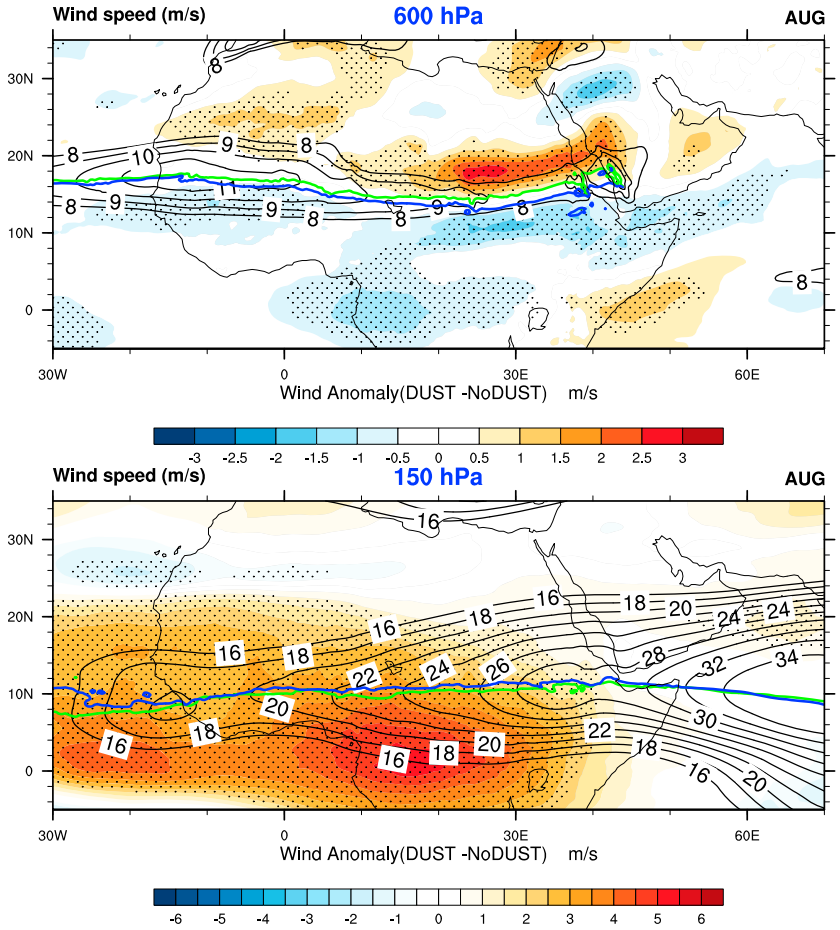

Figure 9. Mean winds (m/s) in August (thin contour lines) and its response (DUST − NoDUST) to DDRF (shaded contours), showing AEJ (600 hPa) and TEJ (150 hPa). The zero contours of the du/dy field near the jets are included to show the axis of the jets, where thick green contour is for the axes in the DUST simulation and the thick blue contour is for that in NoDUST simulation.

that the activity of the intense convective systems follows the seasonal migration of the AEJ, and the peak in the activity occurred immediately poleward of the jet axis. Thus, the predicted northward shift of the mean AEJ axes supposedly moves the intense convective systems farther north and supports heightened activities throughout the region.

TEJ stems from the outflow of strong upper tropospheric anticyclone above the Tibetan plateau [*Koteswaram*, 1958], formed via the elevated solar heating and the latent heat release from the orographic rainfall, and the consequent geostrophic easterly current formation around 150 hPa. Although the generation mechanism is outside the domain of our interest, TEJ has a pivotal role in the MENA climate. This is a good example of the advantage of a GCM over an RCM in properly accounting for two-way interaction between global and regional responses. TEJ is thought to influence the tropical rainfall over the MENA region mainly in three ways: (1) by providing sufficient upper tropospheric shear for the development and maintenance of AEJ and AEW; (2) by the juxtaposition with the surface convergence (e.g., ITCZ), supporting deep convection; and (3) by providing upper air moisture supply. *Nicholson* [2001] showed that the upper troposphere shear, which is dependant on the strength of TEJ, is a key factor in the AEW development. The study also reveals that TEJ links to AEJ by providing sufficient shear near AEJ, which in turn increases the dynamic instability and allows wave development in the vertical direction. Moreover, the region of strong divergence associated with TEJ promotes ascent in the lower and middle troposphere. This further entrains the low-level moisture into higher levels, well into the vicinity of the AEJ [*Nicholson*, 2001]. In effect, TEJ is a crucial component in the entrainment of moisture into the higher levels. In response to DDRF, TEJ strengthens significantly throughout the jet and the axes of the jet shifts slightly farther south (Figure 9b). However, the strengthening in TEJ does not start from the entrance

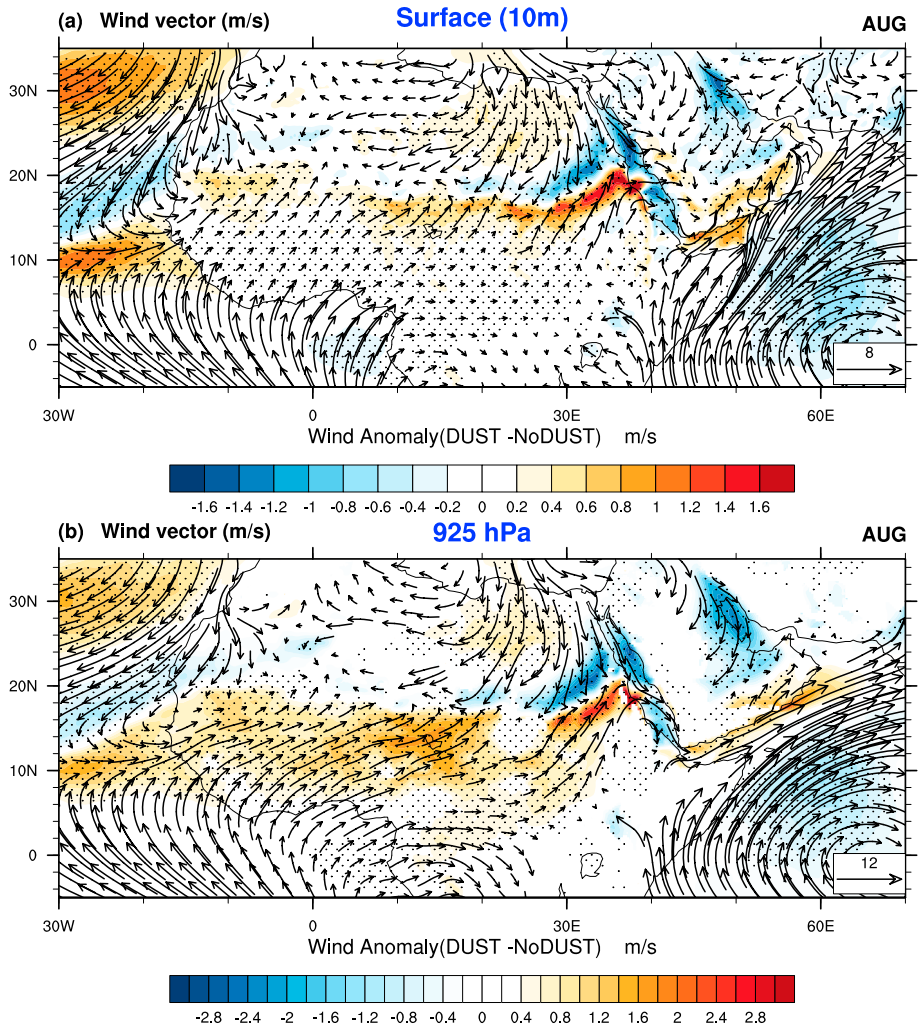

Figure 10. Horizontal wind vectors (m/s) overlaid on the wind speed response (DUST − NoDUST) to DDRF, during August, (a) at surface (10 m) and (b) 925 hPa.

region to the domain (MENA), rather, it starts to strengthen over east Africa and gradually increases toward the Atlantic. Therefore, the strengthening in TEJ could not be a direct effect of DDRF but rather a response to the anomalously heightened convective activities in the region. Conversely, the southward shift in the position of the jet continues from the ISM region. This could be related to the response of ISM to DDRF. The southward shift of the jet axis could displace the juxtaposition of the TEJ with the zone of maximum convection. Though *Hulme and Tosdevin* [1989] associate the southward shift with dry year dynamics over Sudan, it is not well known yet how it influences other regions.

As in the upper atmosphere, there are synoptic-scale circulation features in the lower troposhere with a strong zonal component, which are considered to be key features of the MENA climate. The world's two major monsoons, ISM and WAM, are the major circulations among them. These circulations reside in the proximity of the MENA dust belt, at the eastern and western boundaries, respectively; which is not by coincidence but due to the strong coupling between monsoon and deserts [e.g., *Rodwell and Hoskins*, 1996]. Though these two synoptic systems have their origin partly outside of the MENA domain, especially ISM, they are considered to be some of the major drivers of climate in the region. Therefore, the DDRF impact on these synoptic circulations could effectively feedback the responses inside MENA. Again, this is another good example, showing the advantage of a GCM over RCM for the regional climate sensitivity to some forcings, since GCMs account for the forcing-induced changes outside the domain of interest and its influence back in the domain.

To investigate the two monsoon circulations (WAM and ISM) response, wind speed responses in the lower troposphere are analyzed (Figure 10). The analysis has been done at both surface (10 m) level and at 925 hPa,

to differentiate the orographically induced circulation responses. WAM circulation is enhanced across tropical Africa, especially just south of ITCZ location. This is the major circulation, which brings moisture inland and is considered to be an integral factor for the mean precipitation in tropical Africa. As mentioned before, this circulation has a significant zonal component, which helps to function as the major inland moisture flux mechanism over tropical Africa. The predicted enhancement is consistent with EHP hypothesis, since dust-induced heating over the continent can act as an elevated heat source, which has the potential to enhance the southwesterly onshore flow. Over East Africa the wind response is contrastingly high and has a strong dipole structure. Again, this amplified response over East Africa, could be due to the significant Walker circulation response (Figure 8b) and/or due to the effect of comparatively higher DDRF over this region. Another region showing contrastingly high wind response is the southern border of the Arabian Peninsula, where a small branch of Somali Low Level Jet (SLLJ) intrudes into the land and meets with northeasterlies from the Peninsula. Interestingly, the response of SLLJ, in general, is a weakening, but the land-intruding branch enhances. This indicates that the enhancement in wind speed of the land-intruding jet branch is due to a locally confined heating contrast, while the jet as a whole is influenced by a different mechanism, possibly a gradient outside the domain. This local amplification of wind speed is due to the enhancement of AHL and the dry convection there, due to dust radiative heating. AHL is the major driver for this land-intruding branch of SLLJ.

In conclusion, the northward shift of the ascending branch of Hadley cell, AEJ, and ITCZ along with strengthening of monsoon circulation, supports an enhancement and shift of the tropical rain belt. Comparing with studies that explored the differential atmospheric dynamics in wet and dry years [e.g., *Hulme*, 1996; *Lamb*, 1978; *Janicot*, 1992a] reveals that the DDRF impact on the circulation has similarities to wet year dynamics. In response to DDRF, a northward shift in the AEJ axes and the ITCZ and the strengthening of TEJ is predicted, which are characteristic features of the wet year dynamics. Many of the previous studies have already indicated the possible role of dust in the prolonged desiccation over Sahel [e.g., *Brooks and Legrand*, 2000; *Prospero and Lamb*, 2003; *Yoshioka et al.*, 2007]. Our results strongly suggest that changes in the dust loading could potentially influence the precipitation over semiarid equatorial Africa, and hence, it is essential to include dust radiative effect in the simulations and future projections of this region's climate.

4. Discussion

The tropical rain belt across MENA is not located just under the dust belt; rather, it is located in the proximity of the dust belt, specifically in the southern border of the dust belt. Therefore the responses in the rain belt cannot be immediately linked to the local column radiative-convective balance. The present study suggests that the responses in the rain belt are greatly mediated by the circulation changes induced by the spatially heterogeneous distribution of dust loading and the corresponding heterogeneity in DDRF distribution. That is to say, the dust loading and the corresponding forcing is mainly confined to the NH subtropics (Figure 2), which could potentially influence the local meridional overturning as well as the synoptic circulations, as it perturbs the interhemispheric radiative heating gradient. This is consistently evident from the responses of the climate variables and circulation features in the simulations.

Analysis of the regional Hadley cell (Figures 6 and 7) reveals the substantial responses in the local Hadley circulation strength and position as a response to dust radiative effect. In general, the ascending branch of Hadley cell enhances and shifts to the summer hemisphere as a response to dust radiative effect. These responses are consistent with the previous findings on the strength and location of the Hadley cell. Using simplified models, *Held and Hou* [1980] and *Lindzen and Hou* [1988] showed that, as the heating center moves off the equator, the latitude position separating summer and winter Hadley cell moves farther into the summer hemisphere. Regarding the position of Hadley cells, two major controls have been proposed; equatorial SST pattern and the cross-equatorial tropospheric temperature gradient [*Philander et al.*, 1996; *Tomas et al.*, 1999]. Since we prescribe observed SST in the simulation, the response in the position of the overturning cells solely originates from the changes in the tropospheric temperature gradient that stems from the dust radiative forcing. In the present case, the dust heating confined to the NH subtropics very well functions as an off-equator additional heating source in the lower troposphere. During summer, this dust-induced heating coincides with the solar insolation maxima and thus enhances the interhemispheric temperature gradient primarily driven by insolation. The enhanced interhemispheric heating gradient strengthens and moves the ascending branch of Hadley cell into the summer hemisphere. The northward shift of AEJ also has its root in the same meridional heating gradient, as its development and maintenance greatly depend on the meridional temperature gradient.

Several other modeling as well as observational studies showed the sensitivity of the latitudinal position of Hadley cell and the rain belt to the interhemispheric heating contrast in various contexts, in decadal to glacial-interglacial timescales [*Broccoli et al.*, 2006; *Chiang and Bitz*, 2005; *Mantsis and Clement*, 2009; *Zhang and Delworth*, 2005]. In general, an anomalous northward (southward) shift in the position of tropical rain belt (mentioned as "ITCZ" in many of these studies) are observed in response to NH warming (cooling). The opposing effects of scattering and absorbing aerosols on the tropical rain belt position has also been studied in the past [*Allen and Sherwood*, 2011; *Chung and Seinfeld*, 2005; *Roberts and Jones*, 2004; *Wang*, 2004; *Williams et al.*, 2001]. While the scattering aerosols confined to the NH shift the tropical rain belt farther south due to the weakening of the interhemispheric temperature gradient associated with an enhanced cooling of the NH, absorbing aerosols move it farther north in response to the anomalous radiative heating of the NH. *Wilcox et al.* [2010] observed a northward shift in the tropical rain belt and circulation over the North Atlantic Ocean, in response to summertime Saharan dust outbreaks. The predicted northward shift of the local Hadley circulation and the tropical rain belt in the current study is thus consistent with the previous results and could be attributed to the dust-induced radiative heating in the NH subtropics over MENA. Implicitly, these results also show that the variations in Saharan dust loading could potentially influence Sahel drought episodes along with other proposed mechanisms.

Although the present study predicts an increase in precipitation in response to dust radiative effect over the tropical rain belt, contrasting responses of precipitation were predicted from previous modeling studies, as we discussed in the introduction section. The difference in the dust refractive index and the associated changes in the sign of the DDRF at TOA and the corresponding changes in the atmospheric heating among various models are found to be a major cause of this disparity [*Miller et al.*, 2004a; *Solmon et al.*, 2008]. The studies that predicted an increase in precipitation generally used more absorbing dust, while those that predicted a weakening of precipitation used less absorbing dust. *Solmon et al.* [2008] also showed that the precipitation response to dust forcing is highly sensitive to the dust optical properties using a regional climate model. The dust used in the current experiment assumes a 2.7% hematite content by volume [*Balkanski et al.*, 2007], which lies within the range of previous estimations but at the absorbing end of the range. GFDL simulations for the IPCC AR5 from various models assume the same optical properties for dust [*Donner et al.*, 2011]. However, there is no common consensus on mineral dust absorptivity. It is an ongoing research topic and is a subject of lively debate, which has a wide range of estimated results from various observational and modeling studies [e.g., *Haywood et al.*, 2011; *Otto et al.*, 2009; *Balkanski et al.*, 2007]. However, the current study does not intend to perform experiments on sensitivity of climate response to varying dust absorptivity, which is beyond its scope. Rather, this study exploits the ability of a high-resolution GCM to perform a detailed survey on how global and regional circulations can mediate regional climate response to DDRF over the MENA tropical rain belt, with a reasonably well-estimated dust optical properties. The authors intend to do the sensitivity analysis of these predicted responses to various dust absorptivity as a continuation of the current research.

It is also noteworthy that most of the local hot spots in the climate responses, as seen from surface climate variables (Figures 3–5) and further evidenced by the circulation responses (Figure 10), are over regions with complex orography. The responses in these hot spots are at least twice as large as the responses in the remaining part of the region. These locally amplified responses highlight the importance of incorporating mesoscale forcings such as orography for an accurate simulation of regional climate sensitivity. Coarser resolution GCM simulations generally lack these forcings. But the current simulations with HiRAM take into account these multiscale forcings and effectively reproduce the locally amplified climate features.

5. Summary

We take advantage of the high spatial resolution capabilities of an AGCM, HiRAM, to investigate the regional climate impacts of dust radiative effect on the tropical rain belt in the MENA region. Experiments with dust forcing and those without dust forcing are compared for analyzing the impacts. The significant role of DDRF on the strength and the latitudinal extent of the tropical rain belt has been revealed. In general, dust-induced radiative perturbations tend to increase the precipitation and widen the rain belt northward, resulting in a dipole-like structure in response through most of the region. The semiarid strip situated at the southern edge of the Sahara desert, including Sahel, experiences dramatic enhancement in precipitation. The predicted enhancement is about 20% of mean summer precipitation over this region. This response has a wide range of socioeconomic implications in the context of the Sahel drought.

The study specifically investigates the role of global and regional circulations in mediating the climate response over the region. We found that the major circulation response is in the local Hadley circulation. In response to meridionally asymmetric DDRF, the ascending branch of the local Hadley circulation enhances and shifts farther north into the summer hemisphere. It clearly indicates that the dust-induced radiative heating confined in the NH subtropics effectively functions as a hemispherically asymmetric off-equator heating source and alters the meridional heating gradient. Associated with the shifts in the zonally averaged mean meridional circulation, AEJ, which also depends on the meridional heating gradient, moves farther north by a few degrees. These responses in the circulation features are in phase with the predicted response of the rain belt. WAM is another important circulation feature significantly responsive to dust radiative effects. As a major component of the lower atmospheric zonal circulation, the enhanced WAM circulation extends the moisture supply inland, which is a crucial factor for the tropical rain belt. Overall, the dust induced changes in the tropospheric dynamics are similar to those occurring during wet years. It indicates that the response of MENA dust loading to the climate variability over Sahel could be a possible feedback on the drought episodes. This study highlights the importance of integrating the dust radiative effect for reproducing and projecting the climate of MENA.

Finally, there are some uncertainties in our study. Since experiments are conducted with prescribed SST, they are mostly representative of atmospheric response. The result could change in experiments with an interactive ocean. Similarly, since the dust is prescribed in the current simulation, a feedback of climate response on dust is not considered. The feedback could be either a negative one, due to reduced erodibility associated with the enhanced precipitation toward the deserts [*Yoshioka et al.*, 2007], or a positive one, due to the increased downdraft associated with the northward shift of ITCZ and deep convection [e.g., *Marsham et al.*, 2011]. In addition, the current study is solely devoted to the detailed analysis of the direct radiative effect of dust, though the indirect effect is known to be an equally important factor. Future research needs to include both of these effects for a comprehensive picture of the dust impact on climate.

Acknowledgments

We thank V. Ramaswamy, Ming Zhao, Bruce Wyman, and Christopher Kerr of GFDL for helping to acquire and use HiRAM model. We also thank Paul A. Ginoux of GFDL for providing dust optical properties based on *Balkanski et al.* [2007]. The research reported in this publication was supported by the King Abdullah University of Science and Technology (KAUST). For computer time, this research used the resources of the Supercomputing Laboratory at KAUST in Thuwal, Saudi Arabia. The simulation results and figures are available from the authors upon request. The GPCP Precipitation data provided by the NOAA/OAR/ESRL PSD, Boulder, Colorado, USA, are available at http://www.esrl.noaa.gov/psd/ and the HadCRUT data are available at http://www.metoffice.gov.uk/hadobs/hadcrut3/.

References

Ackerman, S. A., and H. Chung (1992), Radiative effects of airborne dust on regional energy budgets at the top of the atmosphere, *J. Appl. Meteorol.*, *31*(2), 223–233, doi:10.1175/1520-0450(1992)031<0223:REOADO>2.0.CO;2.

Adler, R. F., et al. (2003), The version-2 Global Precipitation Climatology Project (GPCP) monthly precipitation analysis (1979–present), *J. Hydrometeorol.*, *4*(6), 1147–1167, doi:10.1175/1525-7541(2003)004<1147:TVGPCP>2.0.CO;2.

Ahn, H.-J., S.-U. Park, and L.-S. Chang (2007), Effect of direct radiative forcing of Asian dust on the meteorological fields in East Asia during an Asian dust event period, *J. Appl. Meteorol. Climatol.*, *46*(10), 1655–1681, doi:10.1175/JAM2551.1.

Allen, R. J., and S. C. Sherwood (2011), The impact of natural versus anthropogenic aerosols on atmospheric circulation in the community atmosphere model, *Clim. Dyn.*, *36*(9-10), 1959–1978, doi:10.1007/s00382-010-0898-8.

Balkanski, Y., M. Schulz, T. Claquin, and S. Guibert (2007), Reevaluation of mineral aerosol radiative forcings suggests a better agreement with satellite and aeronet data, *Atmos. Chem. Phys.*, *7*(1), 81–95, doi:10.5194/acp-7-81-2007.

Broccoli, A. J., K. A. Dahl, and R. J. Stouffer (2006), Response of the ITCZ to Northern Hemisphere cooling, *Geophys. Res. Lett.*, *33*, L01702, doi:10.1029/2005GL024546.

Brohan, P., J. J. Kennedy, I. Harris, S. F. Tett, and P. D. Jones (2006), Uncertainty estimates in regional and global observed temperature changes: A new data set from 1850, *J. Geophys. Res.*, *111*, D12106, doi:10.1029/2005JD006548.

Brooks, N., and M. Legrand (2000), Dust variability over Northern Africa and rainfall in the Sahel, in *Linking Climate Change to Land Surface Change*, pp. 1–25, Springer, Netherlands, doi:10.1007/0-306-48086-7-1.

Chiang, J. C., and C. M. Bitz (2005), Influence of high latitude ice cover on the marine Intertropical Convergence Zone, *Clim. Dyn.*, *25*(5), 477–496, doi:10.1007/s00382-005-0040-5.

Chung, S. H., and J. H. Seinfeld (2005), Climate response of direct radiative forcing of anthropogenic black carbon, *J. Geophys. Res.*, *110*, D11102, doi:10.1029/2004JD005441.

Chỳlek, P., and J. A. Coakley (1974), Aerosols and climate, *Science*, *183*(4120), 75–77, doi:10.1126/science.183.4120.75.

Cook, K. H. (1999), Generation of the African Easterly Jet and its role in determining West African precipitation, *J. Clim.*, *12*(5), 1165–1184, doi:10.1175/1520-0442(1999)012<1165:GOTAEJ>2.0.CO;2.

Dai, A., P. J. Lamb, K. E. Trenberth, M. Hulme, P. D. Jones, and P. Xie (2004), The recent Sahel drought is real, *Int. J. Climatol.*, *24*(11), 1323–1331, doi:10.1002/joc.1083.

Donner, L. J., et al. (2011), The dynamical core, physical parameterizations, and basic simulation characteristics of the Atmospheric Component AM3 of the GFDL global Coupled Model CM3, *J. Clim.*, *24*(13), 3484–3519, doi:10.1175/2011JCLI3955.1.

Forster, P., et al. (2007), Changes in atmospheric constituents and in radiative forcing, in *Climate Change 2007. The Physical Science Basis*, edited by S. Solomon et al., chap. 2, pp. 129–234, Cambridge Univ. Press, Cambridge, U. K., and New York.

Fox, P., and J. Rockström (2003), Supplemental irrigation for dry-spell mitigation of rainfed agriculture in the Sahel, *Agric. Water Manage.*, *61*(1), 29–50, doi:10.1016/S0378-3774(03)00008-8.

Freidenreich, S., and V. Ramaswamy (1999), A new multiple-band solar radiative parameterization for general circulation models, *J. Geophys. Res.*, *104*(D24), 31,389–31,409, doi:10.1029/1999JD900456.

Anderson, J. L., et al. (2004), The new GFDL global atmosphere and land model AM2-LM2: Evaluation with prescribed SST simulations, *J. Clim.*, *17*, 4641–4673, doi:10.1175/JCLI-3223.1.

Ginoux, P., L. W. Horowitz, V. Ramaswamy, I. V. Geogdzhayev, B. N. Holben, G. Stenchikov, and X. Tie (2006), Evaluation of aerosol distribution and optical depth in the geophysical fluid dynamics laboratory coupled model CM2. 1 For present climate, *J. Geophys. Res.*, *111*, D22210, doi:10.1029/2005JD006707.

Giorgi, F., and L. O. Mearns (1991), Approaches to the simulation of regional climate change: A review, *Rev. Geophys.*, *29*(2), 191–216, doi:10.1029/90RG02636.
Hansen, J., M. Sato, and R. Ruedy (1997), Radiative forcing and climate response, *J. Geophys. Res.*, *102*(D6), 6831–6864, doi:10.1029/96JD03436.
Hansen, J., et al. (2005), Efficacy of climate forcings, *J. Geophys. Res.*, *110*, D18104, doi:10.1029/2005JD005776.
Haywood, J., B. Johnson, S. Osborne, J. Mulcahy, M. Brooks, M. Harrison, S. Milton, and H. Brindley (2011), Observations and modelling of the solar and terrestrial radiative effects of Saharan dust: A radiative closure case-study over oceans during the GERBILS campaign, *Q. J. R. Meteorol. Soc.*, *137*(658), 1211–1226, doi:10.1002/qj.770.
Held, I. M., and A. Y. Hou (1980), Nonlinear axially symmetric circulations in a nearly inviscid atmosphere, *J. Atmos. Sci.*, *37*(3), 515–533, doi:10.1175/1520-0469(1980)037<0515:NASCIA>2.0.CO;2.
Held, I., T. Delworth, J. Lu, K. U. Findell, and T. Knutson (2005), Simulation of Sahel drought in the 20th and 21st centuries, *Proc. Natl. Acad. Sci. U.S.A.*, *102*(50), 17,891–17,896, doi:10.1073/pnas.0509057102.
Horowitz, L. W., et al. (2003), A global simulation of tropospheric ozone and related tracers: Description and evaluation of MOZART, version 2, *J. Geophys. Res.*, *108*(D24), 4784, doi:10.1029/2002JD002853.
Houze, R. A., and A. K. Betts (1981), Convection in gate, *Rev. Geophys.*, *19*(4), 541–576, doi:10.1029/RG019i004p00541.
Hulme, M. (1996), Recent climatic change in the world's drylands, *Geophys. Res. Lett.*, *23*(1), 61–64, doi:10.1029/95GL03586.
Hulme, M., and N. Tosdevin (1989), The tropical easterly jet and Sudan rainfall: A review, *Theor. Appl. Climatol.*, *39*(4), 179–187, doi:10.1007/BF00867945.
Janicot, S. (1992a), Spatiotemporal variability of West African rainfall. Part I: Regionalizations and typings, *J. Clim.*, *5*(5), 489–497, doi:10.1175/1520-0442(1992)005<0489:SVOWAR>2.0.CO;2.
Janicot, S. (1992b), Spatiotemporal variability of West African rainfall. Part II: Associated surface and airmass characteristics, *J. Clim.*, *5*(5), 499–511, doi:10.1175/1520-0442(1992)005<0499:SVOWAR>2.0.CO;2.
Jish Prakash, P., G. Stenchikov, S. Kalenderski, S. Osipov, and H. Bangalath (2014), The impact of dust storms on the Arabian Peninsula and the Red Sea, *Atmos. Chem. Phys. Discuss.*, *14*(13), 19,181–19,245, doi:10.5194/acp-15-199-2015.
Kalenderski, S., G. Stenchikov, and C. Zhao (2013), Modeling a typical winter-time dust event over the Arabian Peninsula and the Red Sea, *Atmos. Chem. Phys.*, *13*(4), 1999–2014, doi:10.5194/acp-13-1999-2013.
Kaufman, Y., D. Tanré, O. Dubovik, A. Karnieli, and L. Remer (2001), Absorption of sunlight by dust as inferred from satellite and ground-based remote sensing, *Geophys. Res. Lett.*, *28*(8), 1479–1482, doi:10.1029/2000GL012647.
Kinne, S., et al. (2005), An aerocom initial assessment-optical properties in aerosol component modules of global models, *Atmos. Chem. Phys. Discuss.*, *5*(5), 8285–8330, doi:10.5194/acp-6-1815-2006.
Konare, A., A. Zakey, F. Solmon, F. Giorgi, S. Rauscher, S. Ibrah, and X. Bi (2008), A regional climate modeling study of the effect of desert dust on the West African monsoon, *J. Geophys. Res.*, *113*, D12206, doi:10.1029/2007JD009322.
Koteswaram, P. (1958), The easterly jet stream in the tropics, *Tellus*, *10*(1), 43–57, doi:10.1111/j.2153-3490.1958.tb01984.x.
Lamb, P. J. (1978), Case studies of tropical Atlantic surface circulation patterns during recent sub-Saharan weather anomalies: 1967 and 1968, *Mon. Weather Rev.*, *106*(4), 482–491, doi:10.1175/1520-0493(1978)106<0482:CSOTAS>2.0.CO;2.
Lamb, P. J., and R. A. Peppler (1992), Further case studies of tropical Atlantic surface atmospheric and oceanic patterns associated with sub-Saharan drought, *J. Clim.*, *5*(5), 476–488, doi:10.1175/1520-0442(1992)005<0476:FCSOTA>2.0.CO;2.
Lau, K., M. Kim, and K. Kim (2006), Asian summer monsoon anomalies induced by aerosol direct forcing: The role of the Tibetan Plateau, *Clim. Dyn.*, *26*(7-8), 855–864, doi:10.1007/s00382-006-0114-z.
Lau, K., K. Kim, Y. Sud, and G. Walker (2009), A GCM study of the response of the atmospheric water cycle of West Africa and the Atlantic to Saharan dust radiative forcing, *Ann. Geophys.*, *27*, 4023–4037, doi:10.5194/angeo-27-4023-2009.
Levin, Z., E. Ganor, and V. Gladstein (1996), The effects of desert particles coated with sulfate on rain formation in the Eastern Mediterranean, *J. Appl. Meteorol.*, *35*(9), 1511–1523, doi:10.1175/1520-0450(1996)035<1511:TEODPC>2.0.CO;2.
Lin, S.-J. (2004), A "vertically Lagrangian" finite-volume dynamical core for global models, *Mon. Weather Rev.*, *132*(10), 2293–2307, doi:10.1175/1520-0493(2004)132<2293:AVLFDC>2.0.CO;2.
Lindzen, R. S., and A. V. Hou (1988), Hadley circulations for zonally averaged heating centered off the equator, *J. Atmos. Sci.*, *45*(17), 2416–2427, doi:10.1175/1520-0469(1988)045<2416:HCFZAH>2.0.CO;2.
Mantsis, D. F., and A. C. Clement (2009), Simulated variability in the mean atmospheric meridional circulation over the 20th century, *Geophys. Res. Lett.*, *36*, L06704, doi:10.1029/2008GL036741.
Marsham, J. H., P. Knippertz, N. S. Dixon, D. J. Parker, and G. Lister (2011), The importance of the representation of deep convection for modeled dust-generating winds over West Africa during summer, *Geophys. Res. Lett.*, *38*, L16803, doi:10.1029/2011GL048368.
Miller, R., and I. Tegen (1998), Climate response to soil dust aerosols, *J. Clim.*, *11*(12), 3247–3267, doi:10.1175/1520-0442(1998)011<3247:CRTSDA>2.0.CO;2.
Miller, R., and I. Tegen (1999), Radiative forcing of a tropical direct circulation by soil dust aerosols, *J. Atmos. Sci.*, *56*(14), 2403–2433, doi:10.1175/1520-0469(1999)056<2403:RFOATD>2.0.CO;2.
Miller, R., J. Perlwitz, and I. Tegen (2004a), Feedback upon dust emission by dust radiative forcing through the planetary boundary layer, *J. Geophys. Res.*, *109*, D24209, doi:10.1029/2004JD004912.
Miller, R., I. Tegen, and J. Perlwitz (2004b), Surface radiative forcing by soil dust aerosols and the hydrologic cycle, *J. Geophys. Res.*, *109*, D04203, doi:10.1029/2003JD004085.
Milton, S., G. Greed, M. Brooks, J. Haywood, B. Johnson, R. Allan, A. Slingo, and W. Grey (2008), Modeled and observed atmospheric radiation balance during the West African dry season: Role of mineral dust, biomass burning aerosol, and surface albedo, *J. Geophys. Res.*, *113*, D00C02, doi:10.1029/2007JD009741.
Mitchell, J., R. Davis, W. A. Ingram, and C. Senior (1995), On surface temperature, greenhouse gases, and aerosols: Models and observations, *J. Clim.*, *8*(10), 2364–2386, doi:10.1175/1520-0442(1995)008<2364:OSTGGA>2.0.CO;2.
Mohr, K. I., and C. D. Thorncroft (2006), Intense convective systems in West Africa and their relationship to the African Easterly Jet, *Q. J. R. Meteorol. Soc.*, *132*(614), 163–176, doi:10.1256/qj.05.55.
Nicholson, S. (2000), Land surface processes and Sahel climate, *Rev. Geophys.*, *38*(1), 117–139, doi:10.1029/1999RG900014.
Nicholson, S., A. Barcilon, and M. Challa (2008), An analysis of West African dynamics using a linearized GCM*, *J. Atmos. Sci.*, *65*(4), 1182–1203, doi:10.1175/2007JAS2194.1.
Nicholson, S. E. (2001), Climatic and environmental change in Africa during the last two centuries, *Clim. Res.*, *17*(2), 123–144, doi:10.3354/cr017123.
Nicholson, S. E. (2009), A revised picture of the structure of the "monsoon" and land ITCZ over West Africa, *Clim. Dyn.*, *32*(7-8), 1155–1171, doi:10.1007/s00382-008-0514-3.

Nicholson, S. E. (2014a), The predictability of rainfall over the greater horn of Africa. Part I. Prediction of seasonal rainfall, *J. Hydrometeorol.*, *15*(2014), 1011–1027, doi:10.1175/JHM-D-13-062.1.

Nicholson, S. E. (2014b), A detailed look at the recent drought situation in the greater horn of Africa, *J. Arid Environ.*, *103*, 71–79, doi:10.1016/j.jaridenv.2013.12.003.

Nicholson, S. E., and J. Grist (2001), A conceptual model for understanding rainfall variability in the West African Sahel on interannual and interdecadal timescales, *Int. J. Climatol.*, *21*(14), 1733–1757, doi:10.1002/joc.648.

Oort, A. H., and J. J. Yienger (1996), Observed interannual variability in the Hadley circulation and its connection to ENSO, *J. Clim.*, *9*(11), 2751–2767, doi:10.1175/1520-0442(1996)009<2751:OIVITH>2.0.CO;2.

Ott, L., B. Duncan, S. Pawson, P. Colarco, M. Chin, C. Randles, T. Diehl, and E. Nielsen (2010), Influence of the 2006 Indonesian biomass burning aerosols on tropical dynamics studied with the GEOS-5 AGCM, *J. Geophys. Res.*, *115*, D14121, doi:10.1029/2009JD013181.

Otto, S., E. Bierwirth, B. Weinzierl, K. Kandler, M. Esselborn, M. Tesche, A. Schladitz, M. Wendisch, and T. Trautmann (2009), Solar radiative effects of a Saharan dust plume observed during SAMUM assuming spheroidal model particles, *Tellus B*, *61*(1), 270–296, doi:10.1111/j.1600-0889.2008.00389.x.

Perlwitz, J., and R. L. Miller (2010), Cloud cover increase with increasing aerosol absorptivity: A counterexample to the conventional semidirect aerosol effect, *J. Geophys. Res.*, *115*, D08203, doi:10.1029/2009JD012637.

Perlwitz, J., I. Tegen, and R. L. Miller (2001), Interactive soil dust aerosol model in the GISS GCM: 1. Sensitivity of the soil dust cycle to radiative properties of soil dust aerosols, *J. Geophys. Res.*, *106*(D16), 18,167–18,192, doi:10.1029/2000JD900668.

Philander, S., D. Gu, G. Lambert, T. Li, D. Halpern, N. Lau, and R. Pacanowski (1996), Why the ITCZ is mostly north of the equator, *J. Clim.*, *9*(12), 2958–2972, doi:10.1175/1520-0442(1996)009<2958:WTIIMN>2.0.CO;2.

Prospero, J. M., and P. J. Lamb (2003), African droughts and dust transport to the Caribbean: Climate change implications, *Science*, *302*(5647), 1024–1027, doi:10.1126/science.1089915.

Prospero, J. M., P. Ginoux, O. Torres, S. E. Nicholson, and T. E. Gill (2002), Environmental characterization of global sources of atmospheric soil dust identified with the nimbus 7 Total Ozone Mapping Spectrometer (TOMS) absorbing aerosol product, *Rev. Geophys.*, *40*(1), 1002, doi:10.1029/2000RG000095.

Putman, W. M., and S.-J. Lin (2007), Finite-volume transport on various cubed-sphere grids, *J. Comput. Phys.*, *227*(1), 55–78, doi:10.1016/j.jcp.2007.07.022.

Ramanathan, V., P. Crutzen, J. Kiehl, and D. Rosenfeld (2001), Aerosols, climate, and the hydrological cycle, *Science*, *294*(5549), 2119–2124, doi:10.1126/science.1064034.

Randles, C., P. Colarco, and A. da Silva (2013), Direct and semi-direct aerosol effects in the nasa GEOS-5 AGCM: Aerosol-climate interactions due to prognostic versus prescribed aerosols, *J. Geophys. Res. Atmos.*, *118*(1), 149–169, doi:10.1029/2012JD018388.

Rayner, N., D. E. Parker, E. Horton, C. Folland, L. Alexander, D. Rowell, E. Kent, and A. Kaplan (2003), Global analyses of sea surface temperature, sea ice, and night marine air temperature since the late nineteenth century, *J. Geophys. Res.*, *108*(D14), 4407, doi:10.1029/2002JD002670.

Roberts, D. L., and A. Jones (2004), Climate sensitivity to black carbon aerosol from fossil fuel combustion, *J. Geophys. Res.*, *109*, D16202, doi:10.1029/2004JD004676.

Rodwell, M. J., and B. J. Hoskins (1996), Monsoons and the dynamics of deserts, *Q. J. R. Meteorol. Soc.*, *122*(534), 1385–1404, doi:10.1002/qj.49712253408.

Rotstayn, L. D., and U. Lohmann (2002), Tropical rainfall trends and the indirect aerosol effect, *J. Clim.*, *15*(15), 2103–2116, doi:10.1175/1520-0442(2002)015<2103:TRTATI>2.0.CO;2.

Schwarzkopf, M. D., and V. Ramaswamy (1999), Radiative effects of CH_4, N_2O, halocarbons and the foreign-broadened H_2O continuum: A GCM experiment, *J. Geophys. Res.*, *104*(D8), 9467–9488, doi:10.1029/1999JD900003.

Schwendike, J., P. Govekar, M. J. Reeder, R. Wardle, G. J. Berry, and C. Jakob (2014), Local partitioning of the overturning circulation in the tropics and the connection to the Hadley and Walker circulations, *J. Geophys. Res. Atmos.*, *119*(3), 1322–1339, doi:10.1002/2013JD020742.

Shindell, D., and G. Faluvegi (2009), Climate response to regional radiative forcing during the twentieth century, *Nat. Geosci.*, *2*(4), 294–300, doi:10.1038/ngeo473.

Shindell, D., M. Schulz, Y. Ming, T. Takemura, G. Faluvegi, and V. Ramaswamy (2010), Spatial scales of climate response to inhomogeneous radiative forcing, *J. Geophys. Res.*, *115*, D19110, doi:10.1029/2010JD014108.

Slingo, A., et al. (2006), Observations of the impact of a major Saharan dust storm on the atmospheric radiation balance, *Geophys. Res. Lett.*, *33*, L24817, doi:10.1029/2006GL027869.

Sokolik, I. N., and O. B. Toon (1996), Direct radiative forcing by anthropogenic airborne mineral aerosols, *Nature*, *381*(6584), 681–683, doi:10.1038/381681a0.

Solmon, F., M. Mallet, N. Elguindi, F. Giorgi, A. Zakey, and A. Konaré (2008), Dust aerosol impact on regional precipitation over Western Africa, mechanisms and sensitivity to absorption properties, *Geophys. Res. Lett.*, *35*, L24705, doi:10.1029/2008GL035900.

Sud, Y. C., E. Wilcox, W.-M. Lau, G. K. Walker, X.-H. Liu, A. Nenes, D. Lee, K.-M. Kim, Y. Zhou, and P. Bhattacharjee (2009), *Sensitivity of Boreal-Summer Circulation and Precipitation to Atmospheric Aerosols in Selected Regions—Part 1: Africa and India*, vol. 27, 3989–4007.

Sultan, B., and S. Janicot (2000), Abrupt shift of the ITCZ over West Africa and intra-seasonal variability, *Geophys. Res. Lett.*, *27*(20), 3353–3356, doi:10.1029/1999GL011285.

Suzuki, T. (2011), Seasonal variation of the ITCZ and its characteristics over Central Africa, *Theor. Appl. Climatol.*, *103*(1-2), 39–60, doi:10.1007/s00704-010-0276-9.

Textor, C., et al. (2006), Analysis and quantification of the diversities of aerosol life cycles within AeroCom, *Atmos. Chem. Phys.*, *6*(7), 1777–1813, doi:10.5194/acp-6-1777-2006.

Thorncroft, C. (1995), An idealized study of African easterly waves. III: More realistic basic states, *Q. J. R. Meteorol. Soc.*, *121*(527), 1589–1614, doi:10.1002/qj.49712152706.

Thorncroft, C., and M. Blackburn (1999), Maintenance of the African easterly jet, *Q. J. R. Meteorol. Soc.*, *125*(555), 763–786, doi:10.1002/qj.49712555502.

Thorncroft, C., and B. Hoskins (1994a), An idealized study of African easterly waves. I: A linear view, *Q. J. R. Meteorol. Soc.*, *120*(518), 953–982, doi:10.1002/qj.49712051809.

Thorncroft, C., and B. Hoskins (1994b), An idealized study of African easterly waves. II: A nonlinear view, *Q. J. R. Meteorol. Soc.*, *120*(518), 983–1015, doi:10.1002/qj.49712051810.

Tomas, R. A., J. R. Holton, and P. J. Webster (1999), The influence of cross-equatorial pressure gradients on the location of near-equatorial convection, *Q. J. R. Meteorol. Soc.*, *125*(556), 1107–1127, doi:10.1002/qj.1999.49712555603.

Tompkins, A., C. Cardinali, J.-J. Morcrette, and M. Rodwell (2005), Influence of aerosol climatology on forecasts of the African easterly jet, *Geophys. Res. Lett.*, *32*, L10801, doi:10.1029/2004GL022189.

Trenberth, K. E., and A. Solomon (1994), The global heat balance: Heat transports in the atmosphere and ocean, *Clim. Dyn.*, *10*(3), 107–134, doi:10.1007/BF00210625.

Trenberth, K. E., D. P. Stepaniak, and J. M. Caron (2000), The global monsoon as seen through the divergent atmospheric circulation, *J. Clim.*, *13*(22), 3969–3993, doi:10.1175/1520-0442(2000)013<3969:TGMAST>2.0.CO;2.

Volz, F. E. (1973), Infrared optical constants of ammonium sulfate, Sahara dust, volcanic pumice, and flyash, *Appl. Opt.*, *12*(3), 564–568, doi:10.1364/AO.12.000564.

Wang, C. (2004), A modeling study on the climate impacts of black carbon aerosols, *J. Geophys. Res.*, *109*, D03106, doi:10.1029/2003JD004084.

Webster, P. J. (2004), The elementary Hadley circulation, in *The Hadley Circulation: Present, Past and Future*, edited by H. Diaz and R. Bradley, pp. 9–60, Springer, Cambridge, U. K., doi:10.1007/978-1-4020-2944-8.

Wilcox, E. M., K. Lau, and K.-M. Kim (2010), A northward shift of the North Atlantic Ocean Intertropical Convergence Zone in response to summertime Saharan dust outbreaks, *Geophys. Res. Lett.*, *37*, L04804, doi:10.1029/2009GL041774.

Williams, K., A. Jones, D. Roberts, C. Senior, and M. Woodage (2001), The response of the climate system to the indirect effects of anthropogenic sulfate aerosol, *Clim. Dyn.*, *17*(11), 845–856, doi:10.1007/s003820100150.

Yoshioka, M., N. M. Mahowald, A. J. Conley, W. D. Collins, D. W. Fillmore, C. S. Zender, and D. B. Coleman (2007), Impact of desert dust radiative forcing on Sahel precipitation: Relative importance of dust compared to sea surface temperature variations, vegetation changes, and greenhouse gas warming, *J. Clim.*, *20*(8), 1445–1467, doi:10.1175/JCLI4056.1.

Yu, J.-Y., and J. D. Neelin (1997), Analytic approximations for moist convectively adjusted regions, *J. Atmos. Sci.*, *54* (8), 1054–1063, doi:10.1175/1520-0469(1997)054<1054:AAFMCA>2.0.CO;2.

Yue, X., H. Wang, H. Liao, and K. Fan (2010), Direct climatic effect of dust aerosol in the NCAR community atmosphere model version 3 (CAM3), *Adv. Atmos. Sci.*, *27*, 230–242, doi:10.1007/s00376-009-8170-z.

Yue, X., H. Liao, H. Wang, S. Li, and J. Tang (2011a), Role of sea surface temperature responses in simulation of the climatic effect of mineral dust aerosol, *Atmos. Chem. Phys.*, *11*(12), 6049–6062, doi:10.5194/acp-11-6049-2011.

Yue, X., H. Wang, H. Liao, and D. Jiang (2011b), Simulation of the direct radiative effect of mineral dust aerosol on the climate at the Last Glacial Maximum, *J. Clim.*, *24*(3), 843–858, doi:10.1175/2010JCLI3827.1.

Žagar, N., G. Skok, and J. Tribbia (2011), Climatology of the ITCZ derived from era interim reanalyses, *J. Geophys. Res.*, *116*, D15103, doi:10.1029/2011JD015695.

Zeng, N. (2003), Drought in the Sahel, *Science*, *302*(5647), 999–1000, doi:10.1126/science.1090849.

Zhang, R., and T. L. Delworth (2005), Simulated tropical response to a substantial weakening of the Atlantic thermohaline circulation, *J. Clim.*, *18*(12), 1853–1860, doi:10.1175/JCLI3460.1.

Zhao, M., I. M. Held, S.-J. Lin, and G. A. Vecchi (2009), Simulations of global hurricane climatology, interannual variability, and response to global warming using a 50-km resolution GCM, *J. Clim.*, *22*(24), 6653–6678, doi:10.1175/2009JCLI3049.1.